Characterization of Medical Ultrasound Transducers using Infrared Imaging

by Dushyanth Giridhar

Bachelor of Engineering in Instrumentation Technology,
July 2006, Visveswaraiah Technological University,
Belgaum, Karnataka, India

A Thesis submitted to the

The Faculty of
School of Engineering and Applied Science
of The George Washington University
in partial fulfillment of the
requirements for the degree of
Master of Science

August 31, 2009

directed by

Matthew Myers, Research Physicist, DSFM, US Food and Drug Administration

Vesna Zderic, Assistant Professor of Electrical Engineering

Dedication

I wish to dedicate this thesis to my parents Jyothi and Giridhar, my grandparents Gangamma and Ramaiah. To my sister Divya, my brother-in-law Hemansu, and my niece Dhriti.

I also wish to dedicate this thesis to my aunts Nagarathna and Poornima, my cousins Priyanka, Sachin, Anush and Amogh, my uncles Krishna and Anand.

Acknowledgements

I wish to thank my parents, sister and relatives for their continual love, patience, understanding and support as I go through life. I would like to thank my mentors at the USFDA, Ronald Robinson and Matthew Myers for their valuable guidance, support and motivation provided, without which this study would not have been possible. To my thesis advisor Vesna Zderic for the guidance and insight provided.

I would like to thank Jack Sliwa from St. Jude Medical for providing the FLIR camera on loan, for carrying out this study. To Leonard Hanssen and Boris Wilthan from National Institutes for Standards and Technology, MD for the technical assistance provided with the emissivity measurements. To Prasanna Hariharan for his guidance and insight provided through out my stay at the USFDA. Thanks to Michael Berman, Diane Nell, Joshua Soneson, Yunbo Liu, Subha Maruvada, Gerald Harris, Larry Grossman and all the other staff members of DSFM at the USFDA for the valuable insights and technical assistance.

Finally, I would like to thank all my friends for the encouragement and support provided.

Abstract

Characterization of Medical Ultrasound Transducers using Infrared Imaging

Characterization of high-intensity focused ultrasound (HIFU) transducers operating at clinical power levels (1000 - 10000 W/cm^2) can be difficult, owing to the possibility of hydrophone damage or sensor interference with the focused beam. This study presents a noninvasive method (no sensors are present in the HIFU field eliminating the issue of interference caused by objects present in the field) for determining the intensity field of a HIFU beam using infrared (IR) imaging. A tissue phantom was used and sonicated with a 1 MHz HIFU transducer. The temperature rise occurring due to attenuation of the ultrasound energy was measured using an infrared camera separated from the surface of the phantom by an air gap.

A commercially available software (PZFlex, Weidlinger Associates Inc., CA) was used to arrive at a finite-element solution to the wave propagation and heat equations within the phantom. By using PZFlex with an iterative inverse technique, the acoustic field giving rise to the IR temperature measurements was computed. From the iterative process, the acoustic power was determined. Power levels of two HIFU transducers were tested and the predicted power values were within about 25% of Radiation force balance measurements. The inverse method based upon infrared thermography shows promise as a tool for quantitatively measuring radiated power for HIFU beams. The temperature measurements taken using the system may also be used to infer the acoustic intensity field and estimate in-vivo temperatures.

Table of Contents

Dedication iii

Acknowledgements iv

Abstract v

Table of Contents vi

List of Figures viii

List of Tables x

List of Symbols and Abbreviations xi

Chapter 1: Introduction 1

1.1 Background and significance 1

1.2 Infrared thermography 6

1.3 Outline of characterization strategy 7

Chapter 2: Experimental Methods and Materials 10

2.1 Experiment with TMM, Teflon, Raz-IR camera in horizontal configuration 11

2.1.1 Equipment and setup 11

2.1.2 Material preparation 12

2.1.3 Experimental procedure 13

2.1.4 Data acquisition 15

2.1.5 Discussion 15

2.2 Experiment with HATMM, Teflon and FLIR camera in vertical configuration 18

2.2.1 Equipment and setup 18

2.2.2 Material preparation 20

2.2.3 Experimental procedure 21

2.2.4 Data acquisition 22

2.2.5 Discussion 22

2.3 Experiment with HATMM & FLIR camera in vertical configuration 25

2.3.1 Equipment and setup 25

2.3.2 Material preparation 25

2.3.3 Experimental procedure 26

Chapter 3: Computational Methods 27

Chapter 4: Results and Discussion 33

Chapter 5: Summary 50

5.1 Summary 50

5.2 Future work 51

5.3 Conclusion 53

References 55

Appendices 58

List of Figures

Figure 1.3.1	Flowchart of the Inverse method used to compare numerical and empirical data	7
Figure 2.1.1	Equipment and setup of experiment with TMM, Teflon and Raz-IR Camera	11
Figure 2.1.2	Transducer to air separation	14
Figure 2.1.3	Asymmetric temperature pattern	17
Figure 2.2.1	Equipment and Setup of experiment with HATMM, Teflon and FLIR camera	18
Figure 2.2.2	HATMM holder setup	20
Figure 2.3.1	Photograph of experimental setup with HATMM, FLIR Camera	25
Figure 2.3.2	Equipment and setup for experiment with HATMM, FLIR Camera	26
Figure 3.1.1	Finite Element model-Wave propagation	28
Figure 3.1.2	Effect of mesh size	30
Figure 3.1.3	Simplified flow chart	31
Figure 3.1.4	Input and Output traces of inverse method	32
Figure 4.1.1	HIFU 6 Location 1, Power 3.37 W	34
Figure 4.1.2	HIFU 6 Location 1, Power 5.20 W	35
Figure 4.1.3	HIFU 6 Location 1, Power 7.46 W	35
Figure 4.1.4	HIFU 6 Power bar chart – Location 1	36
Figure 4.1.5	HIFU 6 Location 2, Power 3.37 W	37

Figure 4.1.6 HIFU 6 Location 2, Power 5.20 W 37

Figure 4.1.7 HIFU 6 Location 2, Power 7.46 W 38

Figure 4.1.8 HIFU 6 Power bar chart – Location 2 38

Figure 4.1.9 HIFU 6 Location 3, Power 3.37 W 39

Figure 4.1.10 HIFU 6 Location 3, Power 5.20 W 40

Figure 4.1.11 HIFU 6 Location 3, Power 7.46 W 40

Figure 4.1.12 HIFU 6 Power bar chart – Location 3 41

Figure 4.1.13 HIFU 2 Location 1, Power 5.37 W 42

Figure 4.1.14 HIFU 2 Location 1, Power 7.71 W 43

Figure 4.1.15 HIFU 2 Location 1, Power 10.48 W 43

Figure 4.1.16 HIFU 2 Power bar chart – Location 1 44

Figure 4.1.17 HIFU 2 Location 2, Power 5.37 W 45

Figure 4.1.18 HIFU 2 Location 2, Power 7.71 W 45

Figure 4.1.19 HIFU 2 Location 2, Power 10.48 W 46

Figure 4.1.20 HIFU 2 Power bar chart – Location 2 46

Figure 4.1.21 HIFU 2 Location 3, Power 5.37 W 47

Figure 4.1.22 HIFU 2 Location 3, Power 7.71 W 48

Figure 4.1.23 HIFU 2 Location 3, Power 10.48 W 48

Figure 4.1.24 HIFU 2 Power bar chart – Location 3 49

List of Tables

Table 1.3.1	Properties of soft tissue and TMM	8
Table 2.1.1	Transducer properties	12
Table 2.1.2	TMM properties	13
Table 2.2.1	HIFU2 and HIFU6 properties	19
Table 2.2.2	HATMM and Water properties	20
Table 2.2.3a	HIFU 2 TAS values	21
Table 2.2.3b	HIFU 6 TAS values	22
Table 4.1.1a	HIFU 6: Difference between RFB and predicted power	49
Table 4.1.1b	HIFU 2: Difference between RFB and predicted power	49

List of Symbols and Abbreviations

u	the acoustic displacement
p	the acoustic pressure
ρ	mean density of a material
c	speed of sound
B/A	the nonlinearity parameter for the medium
c_p	the specific heat of the material
k	the thermal conductivity of a material
W	radiant flux per unit area (Watts/cm^2)
σ	5.673 x 10^{-12} Watts-cm^{-2} K^{-4} (Stephan-Boltzmann constant)
ε	surface emissivity
Q	the heat per unit volume per unit time generated by the absorbed ultrasound
I	acoustic intensity

Chapter 1: Introduction

1.1 Background and significance

Ultrasound is a form of energy consisting of mechanically produced waves of frequencies above the range of human hearing (Bushong et al. 1991). The frequency of these waves typically ranges from 20 kHz to several hundred MHz. Ultrasound is commonly thought of as a diagnostic imaging modality, but therapeutic applications involving High Intensity Focused Ultrasound (HIFU) are rapidly emerging.

HIFU is produced by concave transducers or plane disk transducers with acoustic lenses that focus the ultrasound beam to a focal region on the order of a few millimeters. This focusing results in intensities on the order of 1000 - 10000 W/cm^2 (ter Haar 1995; Vaezy et al. 2001) at the beam focus. The intense energy deposition at the focus results in a rapid temperature rise in a very short time. Temperature increases of the order of 40-60^oC can be achieved within seconds, causing immediate cell necrosis in the targeted region (ter Haar 2001) with minimal damage to the surrounding tissue. The ability of HIFU to deposit high amounts of energy in a small volume has lead to important biomedical applications in the areas of tumor ablation (Kennedy et al. 2003), vessel cauterization (Zderic et al. 2007) and gene activation (Liu et al. 2006).

There are several national and international standards available (IEC 61157 1992, IEC 61161 1992, Preston 2000) to streamline the characterization of ultrasound field generated by diagnostic and imaging ultrasound devices. However, there are no such standards available for measuring HIFU fields. Currently, the majority of HIFU devices

are characterized using methods designed for the low power diagnostic and imaging applications. Fields generated by focused transducers are characterized in water using i) hydrophones and ii) radiation force balances (Shaw and ter Haar 2006).

Spatial and temporal distribution of acoustic parameters can obtained using hydrophones. In this technique, a hydrophone with tip diameter less than 1 mm is scanned across the focal region of the transducer using a tri-axis positioning system. Small steps are used to obtain data in the region of interest. Focal position, peak pressure and beam width of the HIFU beam can be determined from hydrophone scanning. Issues with hydrophone scanning are limited bandwidth, spatial averaging, and damage to the hydrophone (Zhai et al. 2004). To avoid hydrophone damage, the measurements are done at very low power levels.

Direct measurement of total time-averaged acoustic power can be made using a radiation force balance (Maruvada et al. 2007). The transducer to be calibrated is mounted directly above the target, in a water bath. The target may be a highly absorbing target or a reflecting target. Due to the incidence of the ultrasound wave on the target, the target experiences a force. This force is measured using a sensitive balance. Acoustic power can be determined from this measured force. Radiation force can only measure the total acoustic power contained in the beam and is not capable of obtaining the complete acoustic pressure or intensity field (Hariharan 2008).

The above mentioned techniques are well established and widely used to calibrate diagnostic ultrasound devices. The high intensities generated with focused ultrasound introduce limitations such as cavitation. Cavitation is the breaking of a fluid medium

under excessive stresses (Michel 2001). When cavitation occurs, dissolved gases are drawn out of solution producing bubbles, when the acoustic pressure falls below the vapor pressure of the medium (Hariharan 2008). The micro-bubbles can shield the sensor from the HIFU beam, thereby preventing accurate measurement of acoustic parameters. Sensor damage can also occur due to thermal effects due to attenuation of ultrasound and also direct mechanical effects caused by large compressional and tensional forces (Hariharan 2008).

In the regulatory review of new HIFU systems, an important preliminary step is the characterization of the device in a liquid or tissue-mimicking medium. This involves the determination of the total acoustic power and the spatial intensity distribution within the medium. A critical second step is the measurement of temperature rise within a tissue-mimicking material. Due to the destructive potential of HIFU, characterization of the beam at clinically relevant powers can be difficult to perform using standard techniques described in the previous paragraphs. It is therefore worthwhile to pursue noninvasive methods to measure intensity and temperature within the tissue-mimicking material.

HIFU is currently classified as a Class III device, which is subject to Pre-market approval (PMA), by the United States Food and Drug Administration (FDA). Class III devices are those that support or sustain human life, are of substantial importance in preventing impairment of human health, or which present a potential, unreasonable risk of illness or injury. PMA approval is based on a determination of the FDA that the PMA

contains sufficient valid scientific evidence to assure the device is safe and effective for its intended use(s).

Two new techniques currently explored for HIFU intensity or power measurements are described here. Hariharan et al. (2008) developed a non-invasive method for measuring acoustic intensity in a liquid medium, based upon acoustic streaming. The fluid velocity induced in a liquid medium by the absorbed acoustic energy is measured noninvasively using digital particle image velocimetry (DPIV), and related to the acoustic intensity through a mathematical inverse technique. While the streaming method can predict HIFU intensity fields accurately (Hariharan 2008), it cannot produce useful estimates of temperature rise. It is also difficult to apply at high acoustic intensities, where harmonics of the frequency, generated by nonlinear propagation effects must be resolved.

Another new technique explored is the use of Optical-Fiber hydrophones to characterize HIFU beams (Morris et al. 2009). A dual sensing fiber-optic hydrophone that can make simultaneous measurements of acoustic pressure and temperature at the same location was developed for characterizing ultrasound fields and ultrasound-induced heating. The sensor provides a peak noise-equivalent pressure of 15 kPa, an acoustic bandwidth of 50 MHz, and an optically defined element size of 10 μm. As well as measuring acoustic pressure, temperature changes up to 70 °C can be measured, with a resolution of 0.34 °C (Morris). Some advantages of this technique are its ability to withstand high intensity fields, and its ability to simultaneously acquire acoustic waveforms while monitoring induced temperature rises and its small size. The placement

of sensors in the beam may interfere with the incident ultrasound beam resulting in scattering and reflections and other artifacts.

Another commercially available non-invasive method is the Schlieren imaging technique (Harland et al. 2002; Theobald et al. 2004) which works based on changes in the optical index of refraction to qualitatively define the ultrasound field. However, for quantitative evaluation, the pressure field must be reconstructed tomographically. Other than Schlieren imaging, there are no non-intrusive techniques reported in recent literature capable of measuring ultrasound field at high powers.

This thesis describes an alternative noninvasive technique that has the promise for measuring total ultrasound power, intensity distribution, and temperature rise. The technique involves infrared imaging of a material that has been heated by absorbed HIFU energy. A commercially available software (PZFlex, Weidlinger Associates Inc., CA) was used to arrive at a finite-element solution to the wave propagation and heat equations within the phantom. By using a mathematical inverse method, PZFlex was used to compute the acoustic field that gave rise to the temperature measurements made using the IR camera.

1.2 Infrared thermography

Infrared thermography is the measurement of the distribution of radiant thermal energy (one form of heat) emitted from a target surface and converting this to a surface temperature map or thermogram (Infrared Thermography Field Application Guide, EPRI). The three modes of heat transfer are conduction, convection and radiation. IR thermography is most closely related to radiative heat transfer since infrared thermographic instruments measure the radiated thermal energy from the surface of the target (Thermography Field Application Guide).

The Stephan-Boltzmann law is the physical law that relates the energy emitted from a target surface to the surface temperature as follows:

$$W=\sigma\varepsilon T^4 \qquad \text{Equation 1.2.1}$$

where W = radiant flux per unit area (Watts/cm^2) ; σ= 5.673 x 10^{-12} Watts-cm^{-2} K^{-4} is the Stephan-Boltzmann constant; ε= surface emissivity; T= surface temperature in Kelvin. For additional information on Infrared thermography, please refer to "Infrared Thermography Field Application Guide, EPRI". Emissivity of an object is defined as the ratio of the "energy radiated by object" to "energy radiated by a black body".

1.3 Outline of Characterization Strategy

A flow chart summarizing the strategy for noninvasively measuring the acoustic power is contained in Fig. 1.3.1.

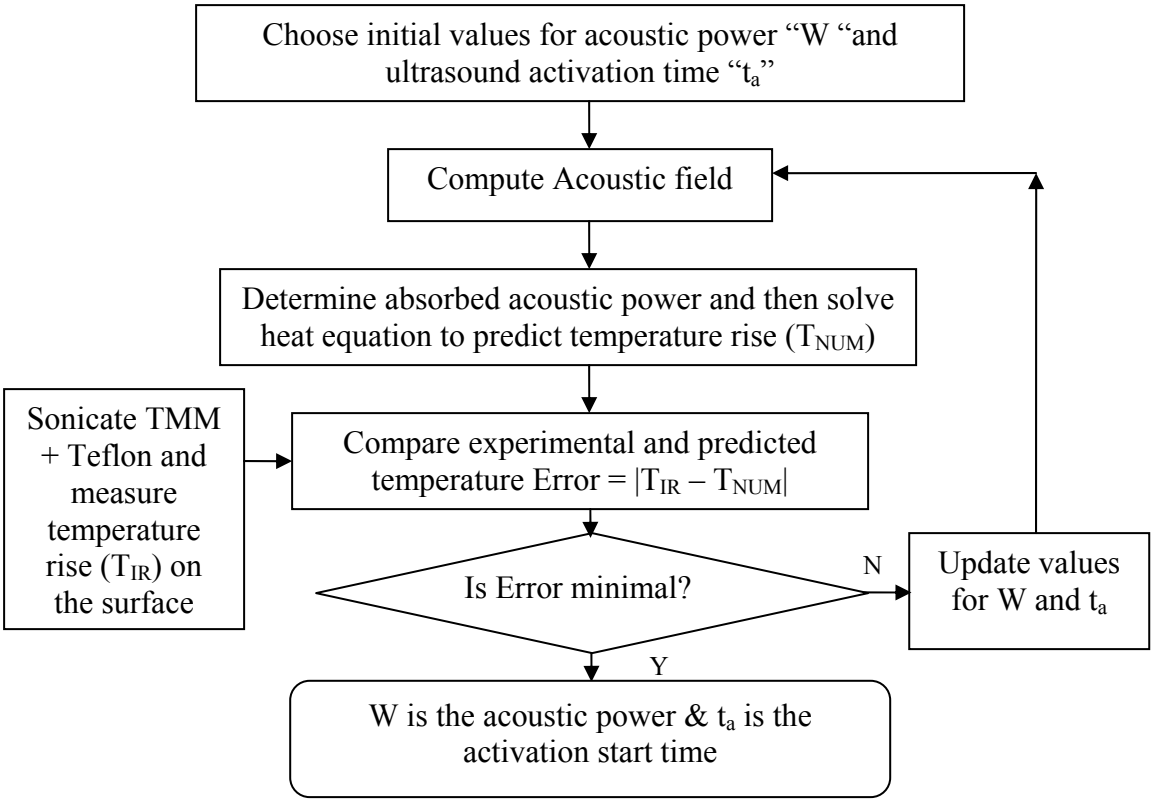

Fig 1.3.1 Flowchart of iterative process used to compare numerical & empirical data

W and t_a are the power and activation time that are adjusted until the experimental and numerical temperature fields best match. The values of W and t_a for which the best match occurs are taken to be the power and activation time.

As shown on the left of the flow chart, the experimental component involves sonicating a tissue phantom and measuring the temperature rise at the surface of the phantom with an IR camera. The hydrogel-based phantom consisted of Gellan Gum,

Calcium Chloride, Potassium Sorbate, Al_2O_3 particles of different sizes, propanol and degassed water. The phantom or tissue mimicking material (TMM) had both thermal and acoustic properties close to that of soft tissue (King et al. 2007). The properties of soft tissue are listed in table 1.3.1 below.

Property	Liver	TMM
Attenuation (dB/cm/MHz)	1.2	1.0
Sound speed (m/s)	1569	1250
Thermal conductivity (W/m.C^0)	0.57	0.58

Table 1.3.1: Properties of soft tissue (Liver) and TMM

The computational component involves simulation of acoustic propagation and attenuation within the phantom, and calculation of the resulting temperature rise. Ultrasound waves in the TMM encounter losses which lead to heating of the material. Real tissue data has a power law dependence on frequency (Szabo, 2004). The heating produced is related to the acoustic intensity and the attenuation of the material as shown in equation 1.3.1.

$$Q = 2 * \alpha * I \qquad \text{Equation 1.3.1}$$

where "α" is the attenuation coefficient of the material and "I" is the intensity of the ultrasound. The intensity of the ultrasound is proportional to the square of the acoustic pressure (equation 1.3.2)

$$I = (p^2) / (2 \rho c) \qquad \text{Equation 1.3.2}$$

where "p " is the acoustic pressure, "ρ" is the density of the material and "c" is the sound speed in the material.

Three experimental apparatuses and protocols were utilized in the process of developing an experimental procedure that could be readily modeled, had minimal heat loss through convective cooling, and had sufficient temporal resolution (30 frames per second). The two preliminary experimental approaches and the final version are

described in the following section. Following the description of the experimental methods, the computational aspects of the procedure are presented. Results of the combined experimental/computational method are then given.

Chapter 2: Experimental Materials & Methods

Several attempts were required to arrive at an experimental setup with which repeatable temperature measurements could be made. The setup consisted of the HIFU transducer sonicating an ultrasound attenuating material and an Infrared camera was used to measure the temperature rise (on the surface of the material opposite to the surface on which HIFU is incident). The third and final experimental setup addresses the issues faced in the first and second setups. The three setups are described in the following pages.

2.1 Experiment with TMM, Teflon & Raz-IR camera in a horizontal configuration

2.1.1 Equipment and setup

The equipment consisted of a Lucite tank with one of the walls having a circular window. Three positioners were attached to an external enclosure made out of Lucite to provide X-Y-Z positioning of the transducer. The infrared camera (Raz-IR, SPI corp., Las Vegas, NV) was attached to an aluminum lab jack/ lift table and placed next to the window of the tank. This allowed for adjusting the height of the IR camera such that the tank window was in its field of view. Right angle clamps were used to position the HIFU transducer behind the window. Figure 2.1.1 below is the schematic of the setup used.

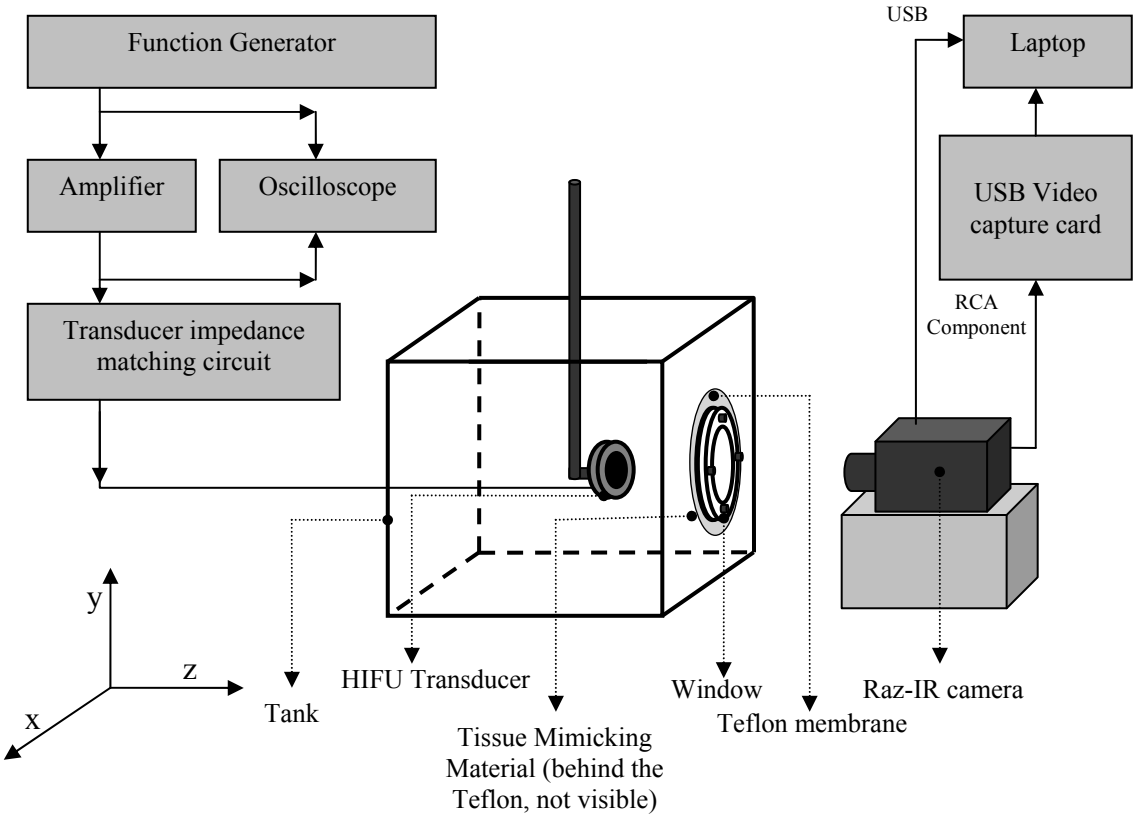

Fig. 2.1.1: Equipment and setup

The transducer properties are listed in table 2.1.1 below. The tank window was sealed using a 0.254 mm Teflon membrane. A cylinder of 1.0 dB/cm/MHz attenuation Tissue Mimicking Material (TMM) was produced using the protocol developed by King et al. (2007) and was inserted into the window and made to lie flush against the inner surface of the membrane.

Transducer properties	
Diameter	6.4 cm
Focal length	6.2 cm
Frequency	1.05 MHz

Table 2.1.1

2.1.2 Material preparation

A circular sheet of 0.254 mm Teflon membrane, with a diameter 2 cm greater than the window diameter was used to seal the tank window. The membrane was introduced to us by engineers from St. Jude Medical. The membrane had two purposes: firstly it was an ultrasound attenuating material which would heat up when sonicated, and the IR camera would measure the temperature on its air-side surface. The second reason was that it was holding the water back in the tank. Care was taken to make sure the sheet was not bent or kinked while attaching it to the tank window. A cylindrical mould with a diameter equal to that of the tank window was used to prepare the TMM. A 1cm high cylinder of TMM was cut using a sharp knife and a guide, and placed behind the membrane. The properties of the TMM are listed below in table 2.1.2. The TMM was used in order to limit the amount of reflected ultrasound (due the abrupt change in the acoustic impedance at membrane-air interface) reaching the HIFU transducer.

TMM properties	
Attenuation	1.0 dB/cm/MHz
Sound speed	1250 m/s
Thermal conductivity	0.58 W/m.C^{o}
Specific heat	3866 kJ/kg.K
Thickness	1.0 cm

Table 2.1.2

2.1.3 Experimental procedure

The tank was filled with fresh de-gassed water. All input and output ports on the amplifier, function generator, oscilloscope, laptop and IR camera were disconnected and allowed to warm up for one hour. The manufacturer of our amplifier, Amplifier Research (Bothell, WA) suggested that the amplifier be allowed to warm up at least an hour in order to avoid oscillating signals. The function generator was set to produce a continuous wave sinusoidal signal at the transducer frequency. The transducer, membrane and camera were aligned such that they were in a straight line, as shown in figure 2.1.1. The focus of the IR camera was checked and adjusted if necessary.

The transducer was moved along the positive Z-axis all the way toward the windowed wall of the tank and made to line up flush against the tank wall. . This position along the Z-axis was noted down using the slider and pointer. An important parameter used throughout the remainder of this thesis is the transducer-to-air separation, or TAS, which is the distance between the transducer face and the air interface (Figure 2.1.2). Accounting for the tank well depth, and using the above position as reference, the distance to be moved back for the required TAS was calculated. The voltage level of the function generator was set by sonicating the TMM and the Teflon membrane for 30

seconds such that the temperature rise was around 30 degrees Celsius above ambient (with a TAS equal to the focal distance).

Three axial locations and corresponding TAS values were considered for this experiment. Location-2 was taken as the TAS for which the highest temperature rise was observed (the end of 30 second sonication, for a given input voltage). The TAS for location-2 of this transducer was around 6.5 cm. The TAS for location-1 and location-3 were about 6.0 cm and 7.0 cm respectively. For location-1, the focus of the transducer was behind the interface, for location-3, the focus of the transducer was beyond the interface, in the air.

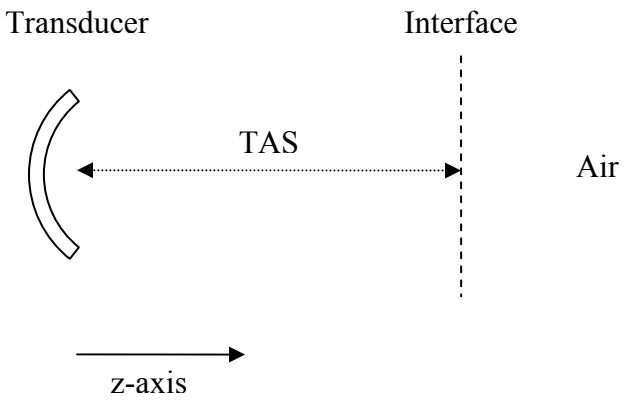

Fig 2.1.2: TAS

The transducer was moved along the Z-axis to obtain the TAS of choice. The transducer was activated for a duration (30 seconds) and the IR images were captured at timed intervals by manually activating the capture button on the IR camera (frame-grab mode). The transducer was switched off and the TMM and membrane were allowed to cool down to room temperature. The camera was then switched to live viewing mode and the transducer was again activated for 30 seconds, and the data was recorded on to the

laptop using the USB video capture device and software interface. The transducer was switched off after 30 seconds and the TMM was allowed to cool down to room temperature before being sonicated again.

2.1.4 Data acquisition

The IR camera's output was connected to a USB-video capture device with an RCA component input. The USB-video capture device was connected to a laptop (IBM T41, IBM Corp.). A video capture software (Showbiz 2 DVD, Arcsoft, Fremont, CA) allowed the recording of the display from the IR camera as an ".mpg" format video file on the laptop hard disk drive. In this "live viewing" mode, the camera had a tracking feature which could track and indicate the pixel with the maximum temperature in its field of view. The camera also had a built-in frame grabbing capability. This allowed us to capture snapshots of the temperature pattern on the surface of the membrane. The captured images were exported to a Microsoft Excel file, which contained information about the temperature of each pixel.

2.1.5 Discussion

Using the "live view" mode of the camera stores each sonication procedure in the ".mpg" video format. In this mode, the camera can only track and display the temperature of the pixel with the maximum temperature. Quantitative temperature information of other pixels was not available from these files. Using the frame-grab mode of the camera can give us temperature information for all the pixels in the captured image. The camera needed to be manually triggered to grab a frame. The frame-grab button had to be pushed

twice, once for the camera to show a preview of the image to be stored and the second time, after a slight delay for it to actually store this image on to its memory. The camera needed approximately 4-5 seconds to be able to capture the next image. The best sampling rate achievable was approximately 1 image for every 5 seconds. This temporal resolution can not give us the temperature information during the first few seconds of sonication when thermal conduction effects are minimal. The slope during the first few seconds of sonication can be seen in the "Results" chapter (Chapter 4),

Another issue is that the manual activation of the "frame-grab" button can result in the movement of the camera, thus any point on the membrane may not appear stationary to the camera. In this setup, the TMM and the membrane were in a vertical position. The TMM had to be slid into place behind the Teflon membrane which would result in a thin layer of water between the TMM and Teflon interface and the thickness of the water column was difficult to measure. In order to accurately model the experimental setup using computational techniques, accurate material properties and dimensions were required. Due to convection currents in the air, in front of the membrane, the heating pattern observed was asymmetric.

The abrupt change in the acoustic impedance at the membrane-air interface would create reflections of the incident ultrasound and lead to standing wave generation (Christensen, 1988). This was observed as variations as high as 50%, in the driving voltage of the transducer. This was a problem because this meant that the ultrasound reflected at the membrane-air interface was interfering with the incident ultrasound beam.

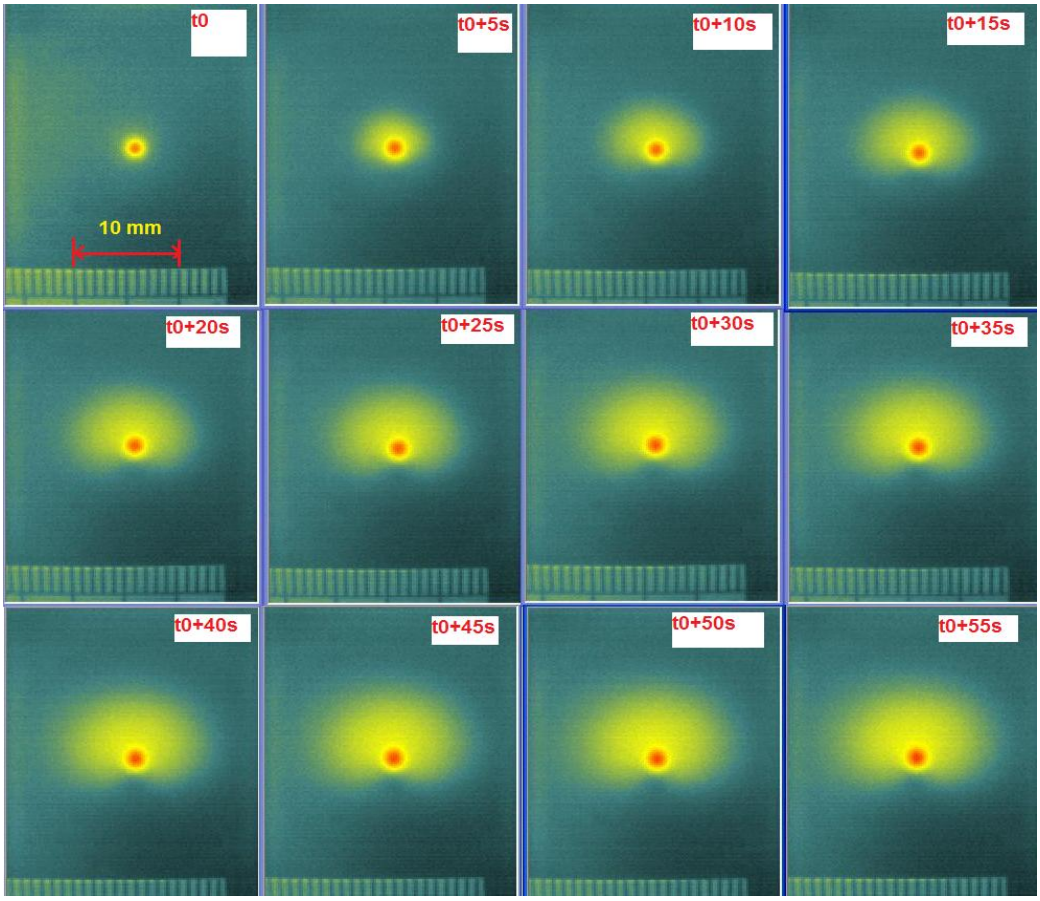

Fig 2.1.3: Asymmetric temperature patterns (a set of images captured using frame-grab feature) seen for Location-2 of the transducer.

A significant drawback of the camera was that it was able to give information about only the pixel with the maximum temperature in the live view mode, and not the other pixels. The freeze-frame mode would give temperature information of all pixels but had low a image capture rate of 1 image in 5 seconds. This was not a good sampling rate as the heating due to ultrasound alone is prominent for the first few tenths of a second.

.

2.2 Experiment with HATMM, Teflon & FLIR camera in vertical configuration

2.2.1 Equipment and setup

The equipment consisted of a Lucite tank with three positioners attached to an external enclosure made out of Lucite to provide X-Y-Z positioning of the transducer. A FLIR SC4000 scientific IR imaging camera was provided on loan by Epicor Medical (subsidiary of St. Jude Medical) through a cooperative Research and Development Agreement (CRADA, 2007) between FDA and Epicor Medical). The infrared camera was mounted on a ring stand in a cantilever fashion using right angle clamps such that the camera would look down into the tank. The camera was calibrated absolutely using a Hart 9133 black body calibrator (Fluke Corp., WA), and for the temperature range of interest, the camera had an absolute temperature uncertainty of $\pm 1^{\circ}$ C for an emissivity value of 0.97. The setup is shown below in figure 2.2.1.

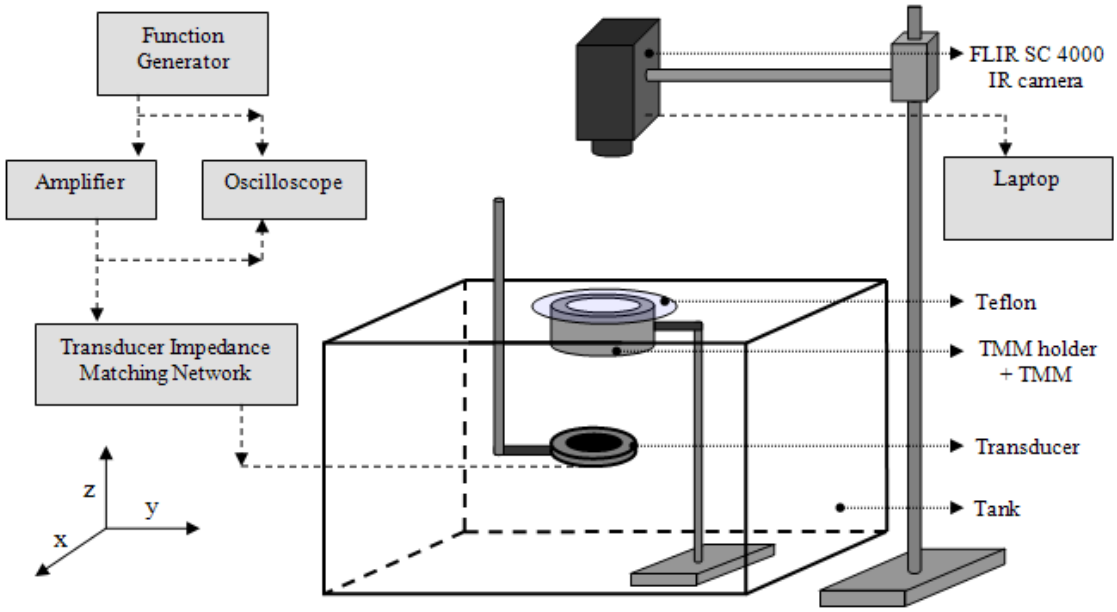

Fig. 2.2.1: Equipment and setup

Right angle clamps were used to position the transducer such that the transducer would face upward toward the camera. Two transducers were used. The properties of the transducers are listed in table below.

Transducer	HIFU2	HIFU6
Frequency (MHz)	1.105	1.155
Focal Length (cm)	10.50	10.00
Diameter (cm)	8.00	10.00

Table 2.2.1: HIFU2 and HIFU6 properties

A cylinder of higher attenuation (1.9 dB/cm/MHz) Tissue Mimicking Material (HATMM) was inserted into a cylindrical plastic holder. The attenuation was increased in order to reduce the generation of standing waves due to reflections from the air interface back into the transducer. The plastic holder was attached to another ring stand and placed in the tank. The HATMM holder was at a height of 30 cm from the floor of the tank to allow movement of the transducer below it such that the TAS could be varied using the Z-axis postioner.

The Teflon membrane was placed on the HATMM surface after applying a thin layer of ultrasound coupling gel on the HATMM surface. The gel was used to act as a coupling medium between the HATMM and Teflon membrane. The presence of air in between the HATMM and membrane would have made the ultrasound reflect at this interface. The top surface and membrane was exposed to air and the IR camera. The camera was at a height of approximately 25 cm from the top of the TMM holder in order to have the surface of the membrane in camera's focus.

2.2.2 Material preparation

The HATMM was created by increasing the Al_2O_3 content in the original TMM preparation protocol by a factor of 10. Its properties are listed below in table 2.2.2.

Property	HATMM	Water
Density (kg/m^3)	1107	998.2
Specific heat (kJ/kg.K)	3876	4182
Attenuation (dB/cm/MHz)	1.9	0.0022
Sound speed (m/s)	1250	1482
Thermal conductivity ($W/m.C^o$)	0.6	0.6

Table 2.2.2: HATMM and Water properties

The thickness of HATMM used was increased from 1 cm to 4 cm. This was done also to reduce generation of standing waves due to reflections at the membrane-air interface. The HATMM and holder setup is shown below in figure 2.2.2.

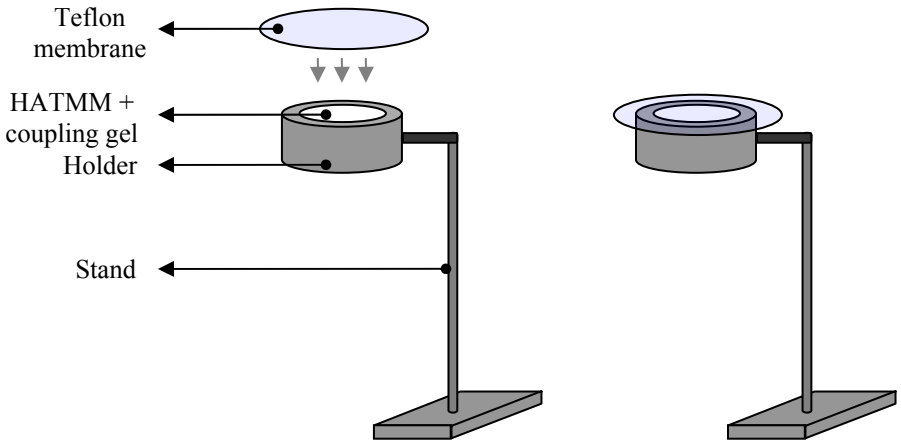

Fig 2.2.2: TMM holder setup

A thin layer of ultrasound coupling gel was applied on the top surface of the TMM. An 8 cm diameter circular sheet of 0.254 mm Teflon sheet was cut using a razor blade and was carefully placed on the TMM and a soft roller was used to remove excess coupling gel and any trapped air bubbles under the membrane.

2.2.3 Experimental Procedure

The level of the transducer was checked with a spirit level and then lowered into the tank. The ring stand with the HATMM, coupling gel, and Teflon membrane were slowly lowered into the tank and the level of the holder and TMM surface was checked with a spirit level to ensure normal incidence of the ultrasound through the TMM and on the membrane. All input and output ports on the amplifier, function generator, oscilloscope, laptop and IR camera were disconnected and allowed to warm up for one hour. The function generator was set to produce a continuous wave sinusoidal signal at the transducer frequency.

The voltage level of the function generator was set by sonicating the TMM and the Teflon membrane for 30 seconds such that the temperature rise was around 30 deg. C above ambient (with a TAS equal to the focal distance). The motivation for using 30 deg. C rise above ambient was to keep safely away from the boiling point of the tissue-mimicking material during the 30-second exposures. The boiling point of the tissue mimicking material was not precisely known, but it was between 90 and 100 deg. C.

The three target axial locations and the associated TAS values are shown below in tables 2.2.3 a, for the two transducers HIFU2 and HIFU6

HIFU 2: TAS values		
Location 1	Location 2	Location 3
10.00 cm	10.75 cm	11.50 cm

Table 2.2.3a

HIFU 6: TAS values		
Location 1	Location 2	Location 3
9.50 cm	10.00 cm	10.50 cm

Table 2.2.3b

The transducer was then moved along the Z-axis to the required location. The TMM and Teflon membrane were sonicated for 30 seconds and the IR camera recording was started to capture the developing heating pattern on the membrane surface. The transducer was switched off and the TMM and membrane were allowed to cool down to room temperature. Temperature data was obtained for HIFU2 and HIFU6 at the three locations, for three different power levels at each location.

2.2.4 Data acquisition

The camera was operated via the software interface, ThermaCam Researcher Pro. The duration of recording and frame rate could be altered using the software interface. The camera was set to record IR images at the maximum rate possible (approximately 30 frames per second) for a duration of 30 seconds to save the data onto the laptop hard disk drive.

2.2.5 Discussion

The best frame rate achievable with this camera is about 30 frames per second. This gave us a much better temporal resolution than that of the previous IR camera. The heating pattern observed was symmetric due the orientation of the HATMM-Teflon

surface and the IR camera. In the previous setup, convection currents of air would sweep across the temperature pattern, causing it to be skewed from top to bottom. Here, any air motion is away from the plane of observation, not causing any asymmetries.

The standing wave generation was minimized as the variation in input power was reduced to less than 10%. One of the issues that were faced is that the coupling gel used between the membrane and the TMM was getting liquefied after repeated exposure to heating. This lead to creation pockets of water under the membrane. The thickness of the water layer is required for the finite element software to model all the interfaces and layers accurately, and measuring the thickness of the layer of water under the membrane is difficult.

A second issue involved the Teflon membrane. The membrane was still used in this setup as in the previous setup, even though there was no need for it to retain the water (as in the previous case) or because of its ultrasound attenuation properties. The relatively low emissivity of the membrane was a potential problem.

An emissivity value less than 90% meant the IR camera would underestimate the temperature of the object (Infrared Thermography Field Application Guide). Emissivity measurements carried out at National Institute of Standards and Technology (NIST), MD revealed that the value of emissivity for our HATMM was measured to be 97% for the FLIR camera's operating wavelength range (Hanssen, 2009). The emissivity of the 0.254 mm Teflon membrane was found to be varying over the camera's wavelength range (3-5 μm). Since the emissivity of the HATMM was greater than 95%, and the HATMM was itself attenuating ultrasound to generate a measurable temperature rise, it was decided that the Teflon membrane would not be used in the follow up experiments. Eliminating

the use of the Teflon membrane also meant that the mathematical simulations could be simplified further as there was no need to simulate the additional interfaces due to the Teflon membrane and the liquefied coupling gel. The experimental setup without the Teflon membrane, described in the next section was the final setup.

2.3 Experiment with HATMM & FLIR camera in vertical configuration

2.3.1 Equipment and Setup

The setup was the same as the one described in Section 2.2.1 but the Teflon membrane and the ultrasound coupling gel were not used. The IR camera would directly image the top surface of the HATMM as shown in figures 2.3.1 & 2.3.2 below.

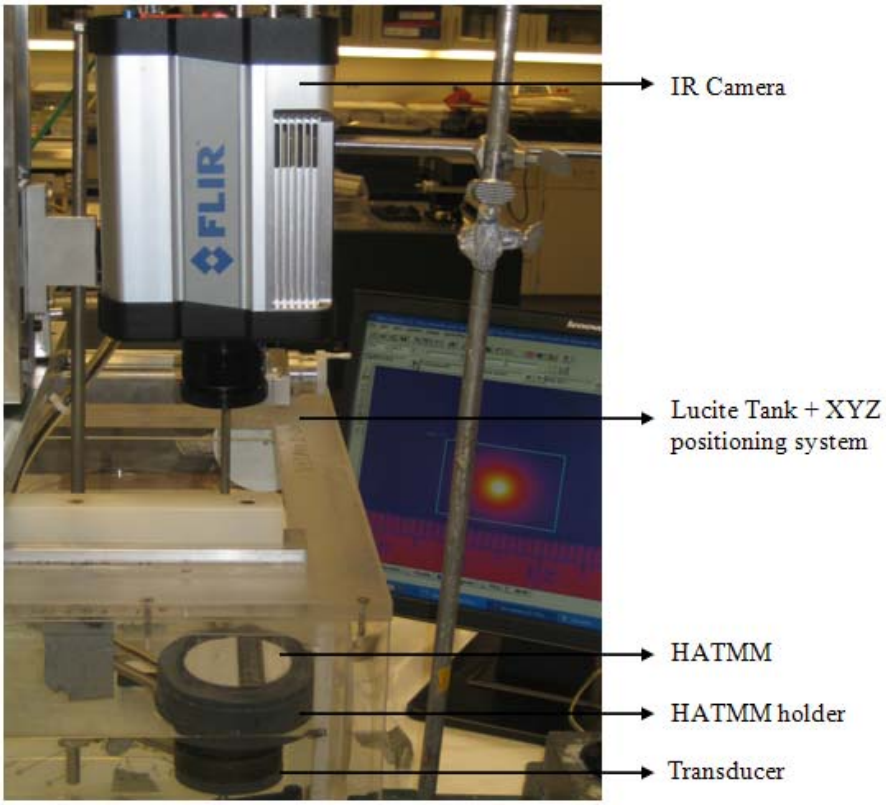

Fig 2.3.1: Photograph of Equipment and setup

2.3.2 Material preparation

The HATMM was placed in the holder as described in section 2.2.2 without the Teflon membrane and the coupling gel.

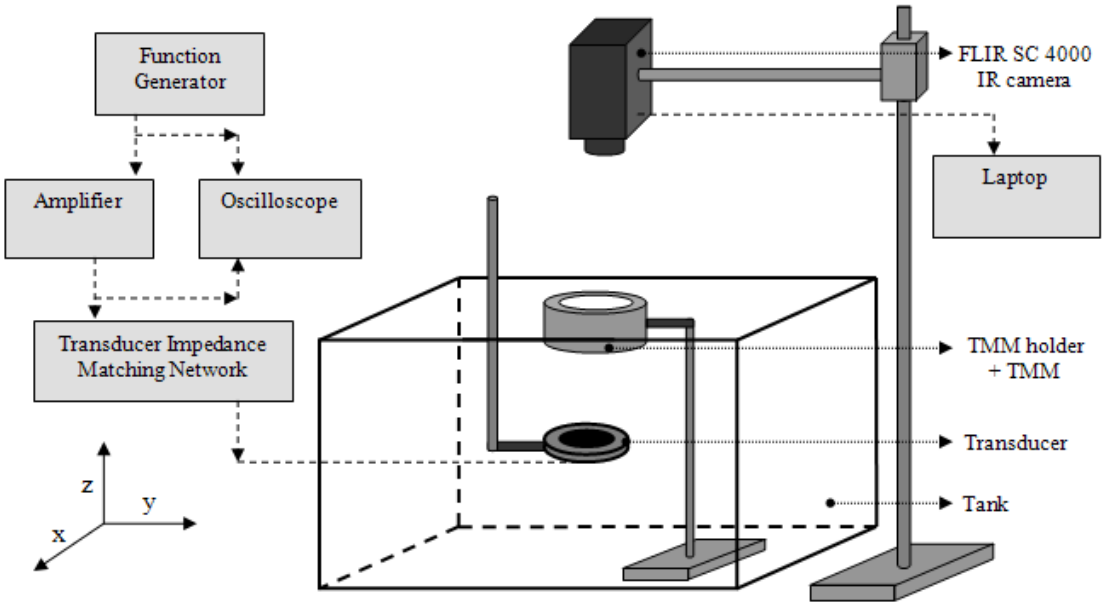

Fig 2.3.2: Equipment and setup

2.3.3 Experimental Procedure

The stand with the holder and HATMM were slowly lowered into the tank and the level of the holder and HATMM surface was checked with a spirit level to ensure normal incidence of the ultrasound through the HATMM. As described in section 2.3.3, three locations were considered for this experiment. The TAS values for the two transducers are listed in tables 2.2.3a and 2.2.3b. Temperature data was obtained for HIFU2 and HIFU6 at the three locations, for three different power levels at each location.

The electrical power is proportional to the product of the input voltage and the current flowing in a system. That is,

Electrical Power = V * I or Electrical Power α V^2

The transducers used in the study had an efficiency of 90% or higher, hence the acoustic power generated by these transducers was around 90% of the electrical power.

Chapter 3: Computational Methods

The characterization strategy (Figure 1.3.1) requires numerical simulation of wave propagation within the experimental geometry. The finite-element software PZFlex (Weidlinger Associates, Menlo Park, CA) was used to perform the simulations. PZFlex solves the conservation of momentum equation (equation 3.1) and a nonlinear constitutive relation (equation 3.2):

$$\rho \frac{\partial^2 u}{\partial t^2} = -\nabla p \qquad \text{Equation 3.1}$$

$$p = -\rho c^2 [\nabla \cdot u + \frac{1}{2}\frac{B}{A}(\nabla \cdot u)^2] \qquad \text{Equation 3.2}$$

Here u is the acoustic displacement and p is the acoustic pressure. The quantities ρ and c are the mean density and speed of sound. The quantity B/A is the nonlinearity parameter for the medium. PZFlex also solves the energy equation,

$$\rho c_p \frac{\partial T}{\partial t} = k\nabla^2 T + Q, \qquad \text{Equation 3.3}$$

where c_p is the specific heat, k is the thermal conductivity, and Q is the heat per unit volume per unit time generated by the absorbed ultrasound.

PZFlex has been tested and validated in previous projects at the FDA, including a study into safety issues when a HIFU beam is incident upon a bone surface (Nell and Myers 2009). Conditions for the bone study were similar to those of the present study, in that reflection of the beam off of the bone surface resulted in a rapidly (in space) varying interference field between the incident and reflected waves. In the present study, a rapidly oscillating field resulting from the interference of the incident beam and the one

reflected off of the air interface must be resolved computationally. Input to PZFlex includes the acoustic and thermal properties of the media involved. Properties of the HATMM and water are listed in Table 2.2.2. The computational geometry with relevant boundary conditions is shown in figure. 3.1.1 below. To simulate the spherically focused transducer, the transducer face pressure was specified along the Y axis in Fig. 3.1.1.

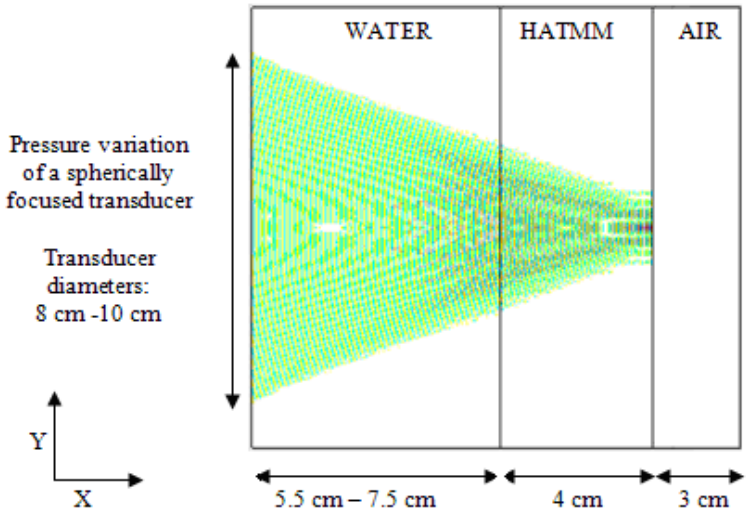

Fig. 3.1.1: Finite Element Model - Wave propagation

To accomplish focusing, the phase of the pressure wave is changed by an amount of "$r^2/ (2\ c_o\ d)$" where r is the radial distance from the center of the transducer, c_o is the speed of sound in the medium of interest and d is the focal distance. In our case, sound propagates through multiple media and a weighted average sound speed is used. The details can be found in the PZFlex input file attached as Appendix A. The hardware requirements for PZFlex are listed as below.

- 64-bit dual-core, dual-processor system (AMD or Intel)
- 4-GB RAM (minimum)
- 500-GB hard drive
- NVIDIA/ATI 256-MB graphics card with Open-GL support
- Minimum display resolution of 1280 x 1024

The time needed to run one simulation of the wave propagation file (Appendix A) was about 24 hours. The time required to run the heating file (Appendix A) was about 2 minutes.

For application of the finite-element method, the geometry was divided into rectangular elements. The size of the elements can be obtained from the ratio of the acoustic wavelength and the number of elements. The wavelengths used in the simulation were on the order of a millimeter. The number of elements per acoustic wavelength was increased, starting at 20, until further increases resulted in no change of temperature at the end of the simulated sonication. It was determined that 60 points per wavelength were required (80 points yielded essentially the same results) in order to resolve the rapidly varying interference field at the TMM/Air boundary. Fig. 3.1.2 summarizes the study into the effect of mesh size.

The iterative process shown in Figure 1.3.1 involves refinement of the transducer power and activation start time of HIFU beam. The signal generator driving the transducer was not synchronized to the infrared camera; hence, the camera began recording a few tenths of a second, after transducer activation. Since this activation time was unknown, it was determined during the inverse procedure. In general, the inverse algorithm requires PZFlex to be run any time the transducer power is updated. However, it was found that at relatively low powers (up to 17 W), the transducer power simply scaled the temperature by the same amount. The procedure for shifting the IR measurements and scaling the PZFlex power values can be found in Appendix B.

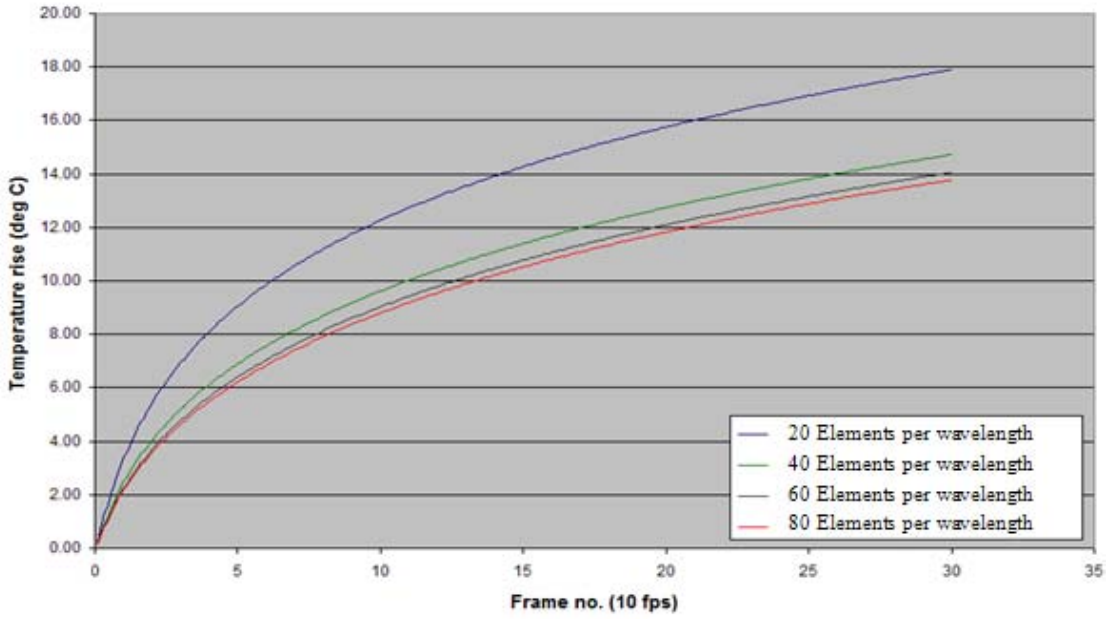

Fig. 3.1.2: Effect of Mesh size (PZFlex temperature trace - HIFU 6, Location 3 - center of hot spot)

To take advantage of this linear behavior, whenever the power was adjusted by a factor, the PZFlex temperature was multiplied by the same factor. The iterative procedure commenced by first establishing a range of time shifts "t_a" and transducer powers W to be considered. The ranges considered were: $0 \leq t_a \leq 9$ data points (each data point was 0.1 second) and 0.001 Watt $\leq$ W $\leq$ 12.1 Watts. The procedure involved consideration of all possible values in these ranges, with t_a interval broken up into 10 values and W incremented by 0.001 W. The flowchart of Fig. 1.3.1 is simplified to the one in Fig. 3.1.3 below.

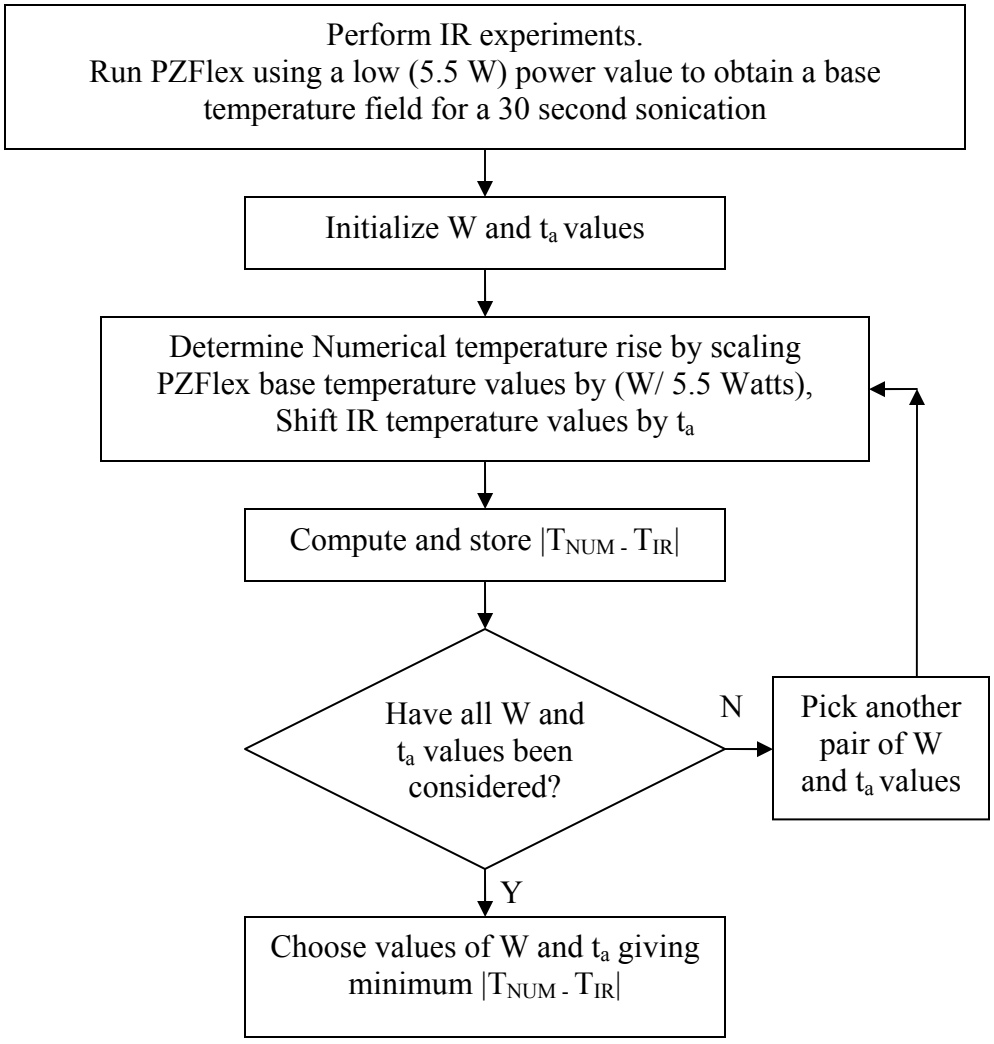

Figure 3.1.3: Simplified flow chart

Fig. 3.1.4 below shows the input (Un-shifted IR data and Un-scaled PZFlex data) and output (Time-shifted IR data and Scaled PZFlex data) of the inverse method together. The output of the inverse method consisted of two temperature traces, and an estimate of the difference between the two curves. The first output curve is the infrared temperature measurements shifted in time (in steps of a tenth of a second, from 0 to 1 second, due to the delay in the camera recording) by the inverse method, in order to best match the computational curve. The computational curve was generated by PZFlex, with the power scaled by the inverse method to match the shifted empirical values.

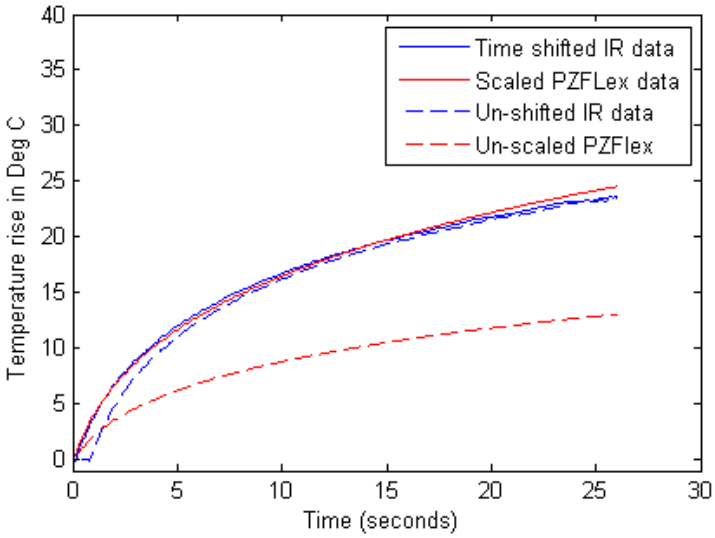

Fig 3.1.4: Input and Output of inverse method

The error value was the RMS average of the temperature values for times 1 second to 26 seconds, sampled at 1 second interval. The experimental transducer activation time was found to vary only within the first second of activation. The upper time limit was taken to be 26 seconds, so that time shifts performed by the inverse method would not go beyond the end of the 30-second data set. The RMS value returned by the inverse method was taken to be the error in the power measurement. This value was typically much larger than the error (average was around 23%) for the three trials of a given experiment, which measured the reproducibility of the experiments and was usually less than 1%.

Chapter 4: Results and Discussion

Infrared measurements of temperature were made at the 3 transducer axial locations, using the 3 powers at each location. These 9 experiments were performed 3 times each. This protocol was used for transducers HIFU2 and HIFU6. Following data acquisition, the inverse method described in the previous section was used to determine the radiated acoustic power in each experiment. The powers derived in the iterative process were compared with powers measured by a radiation-force balance (RFB) technique (Maruvada et al. 2007).

Figure 4.1.1 shows the numerical and empirical temperature traces for the case of HIFU6-location 1, at a power level of 3.37 Watts. The optimization routine yields empirical and numerical traces which are very close to one another; the temperature rise (initial slope of the trace) is comparable during the initial heating period of around a second, as well as later times (after 1 second) where conduction becomes important. A close fit can also be seen in Figure 4.1.2, where the power has been increased to 5.20 Watts, though the curves are not quite as similar as seen in Figure 4.1.1. A slight divergence (up to 1 deg. C) can be seen at later times. For the highest power of 7.46 W, the empirical and numerical curves have moved further apart (up to 2 deg. C); the empirical curve shows more rapid heating initially, followed by a slower rate of heating at longer times. The acoustic power predicted by the inverse method is shown in Figure 4.1.4, along with radiation force balance (RFB) power measurements.

For HIFU6-location 1 (Figures 4.1.1 – 4.1.4), the power values based upon the inverse method exceed RFB values at each power level. Also, the inverse method's predictions become more accurate with increasing power. The RFB value is about 25% below the value determined by the inverse method at the lowest power, 21% below at the intermediate power, and 16% below at the highest power. As noted above, the error estimate on the inverse method power derives from the RMS error between the numerical and experimental temperature traces. The uncertainty in the RFB measurements is approximately 10% (Maruvada et al. 2007).

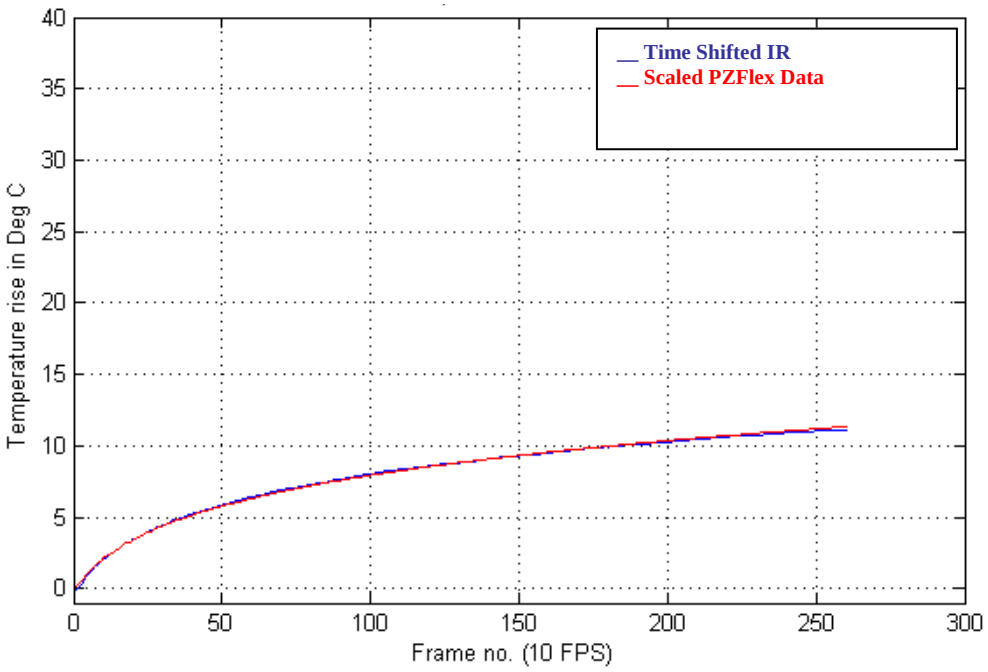

Fig. 4.1.1: Temperature trace for center of hot spot – HIFU6, Location 1, Power 3.37 W

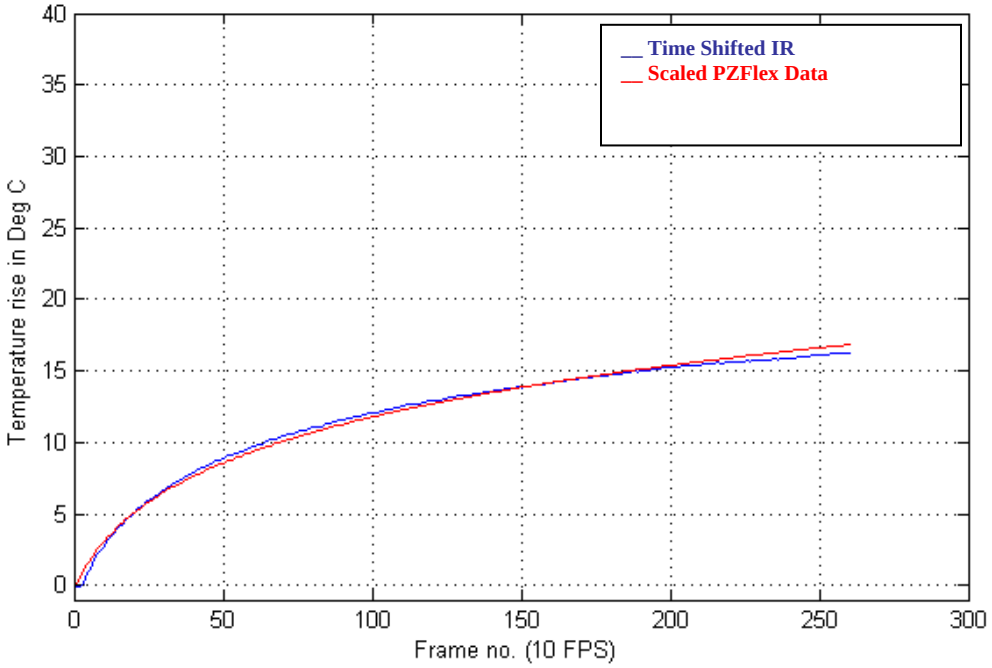

Fig. 4.1.2: Temperature trace for center of hot spot – HIFU6, Location 1, Power 5.20 W

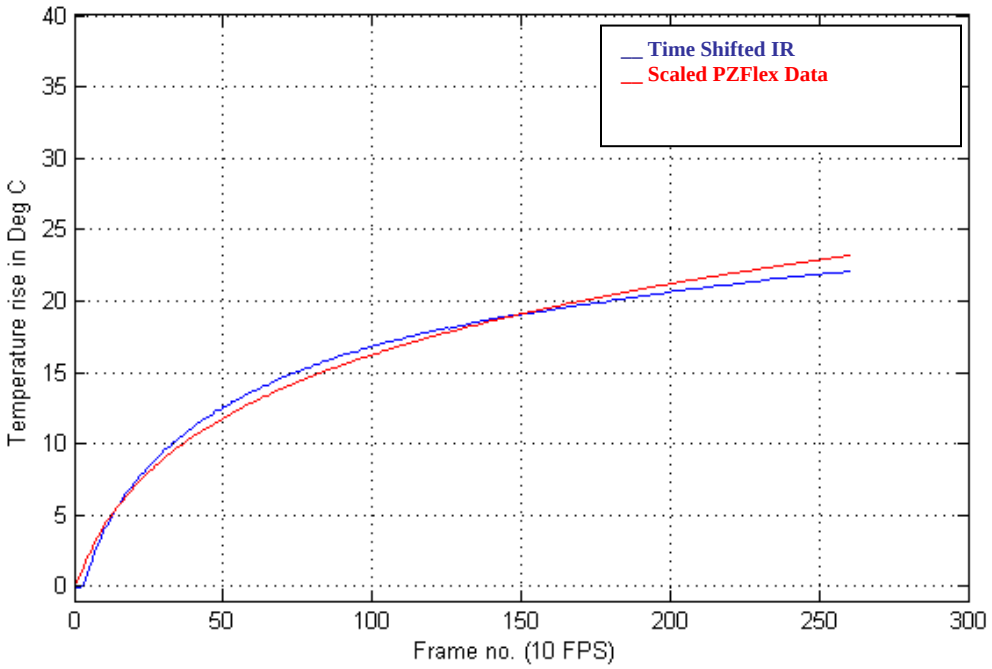

Fig. 4.1.3: Temperature trace for center of hot spot – HIFU6, Location 1, Power 7.46 W

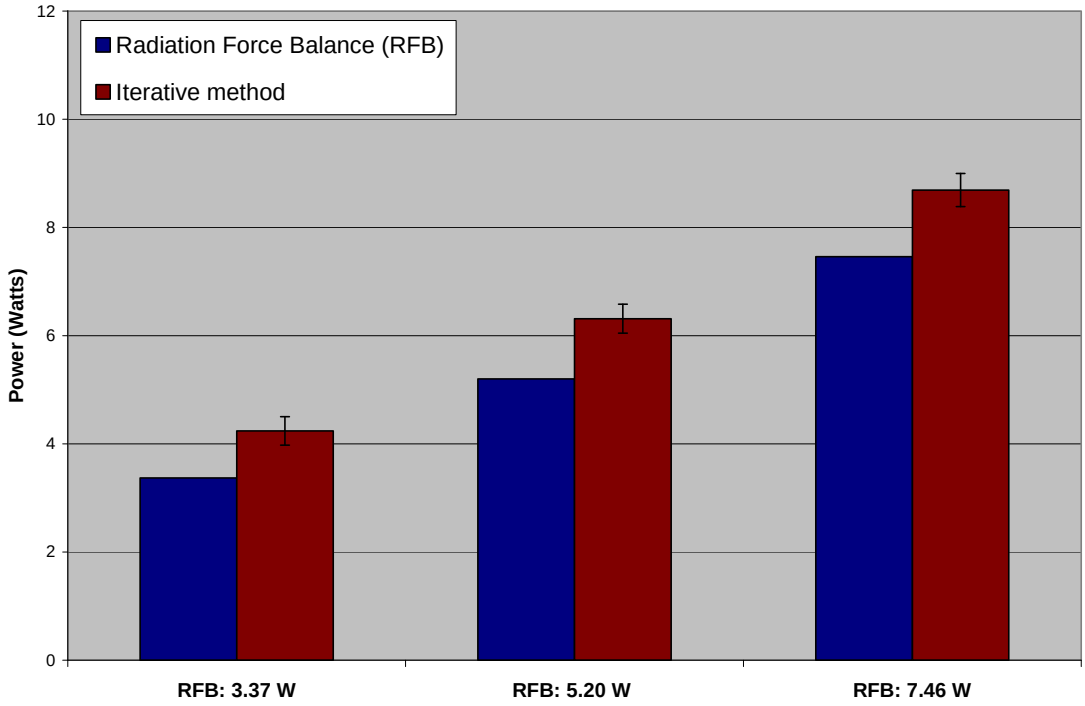

Fig. 4.1.4: Power bar chart for center of hot spot – HIFU6, Location 1

For HIFU6-location 2 (Figures 4.1.5 to 4.1.8), the agreement between the computational and empirical temperature traces is not as close as curves for location 1. In each case, the initial heating rate is higher for the infrared data, but subsequent heating is not as intense as that predicted by PZFlex. The power values predicted by the inverse method, shown in Figure 4.1.8, again exceed the RFB values at each power level. Also, the inverse method and RFB power predictions become closer as the power is increased.

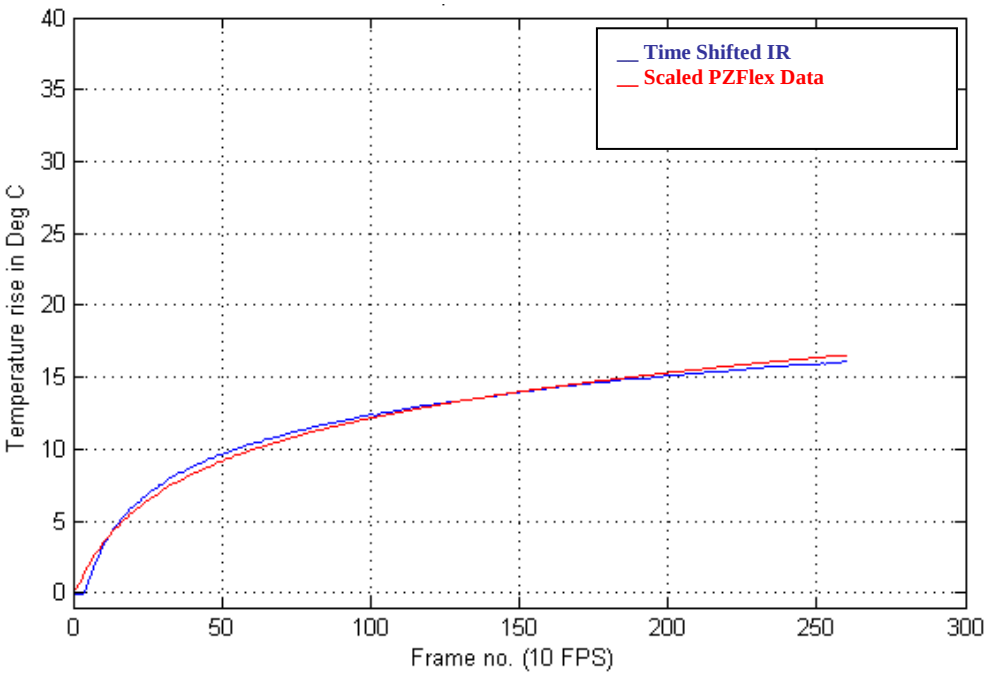

Fig. 4.1.5: Temperature trace for center of hot spot – HIFU6, Location 2, Power 3.37 W

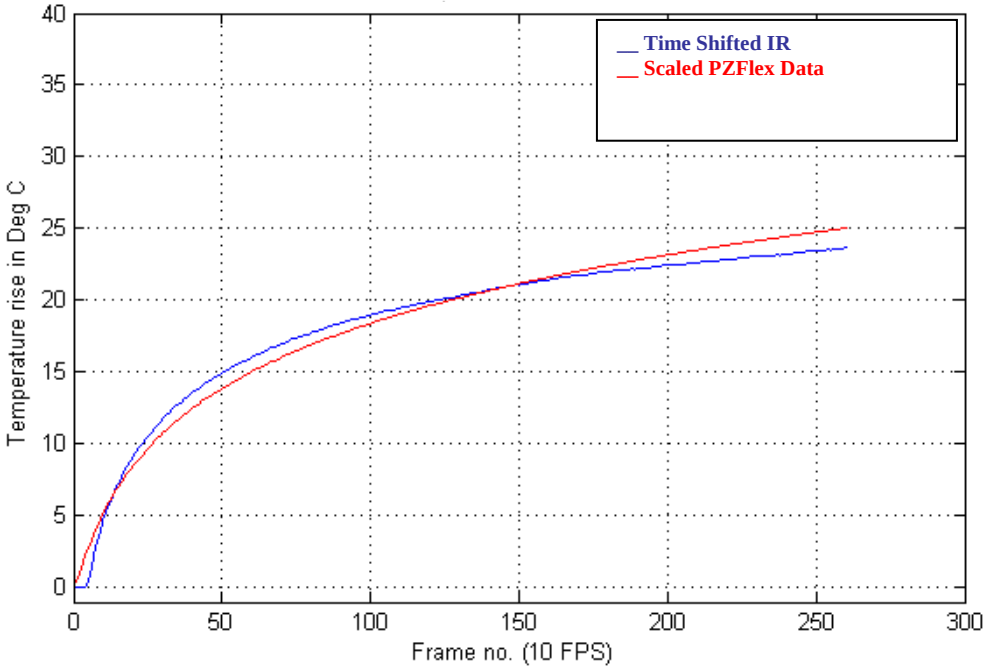

Fig. 4.1.6: Temperature trace for center of hot spot – HIFU6, Location 2, Power 5.20 W

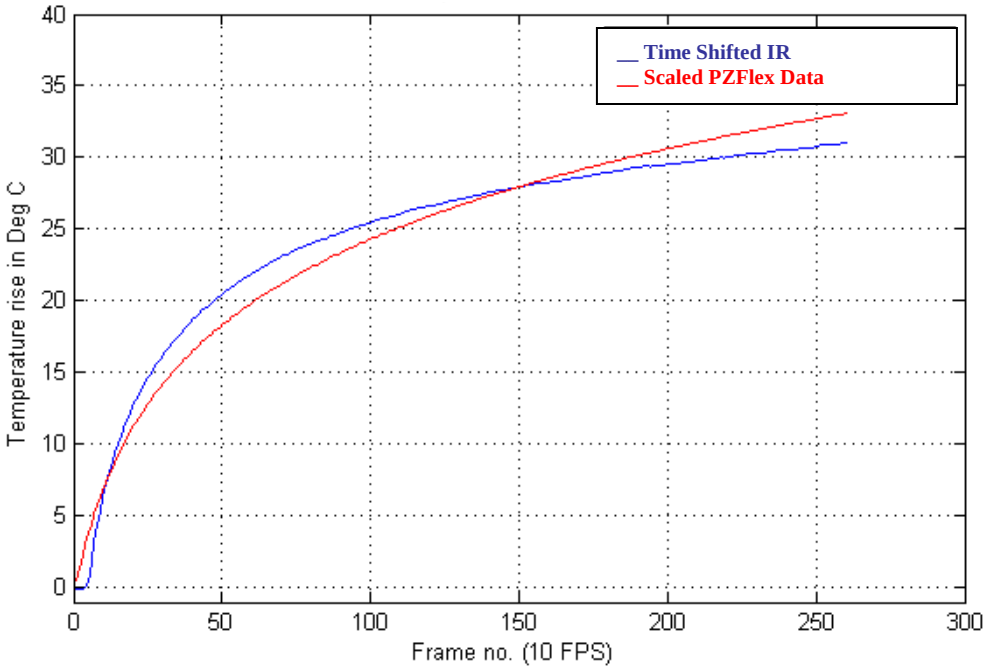

Fig. 4.1.7: Temperature trace for center of hot spot – HIFU6, Location 2, Power 7.46 W

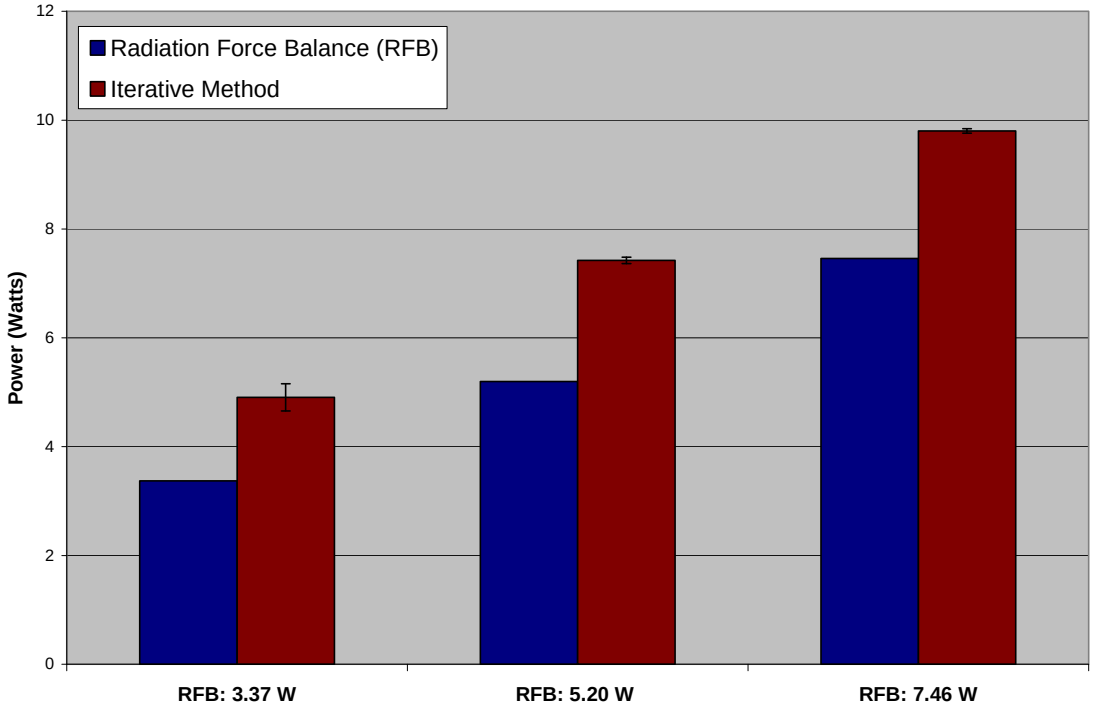

Fig. 4.1.8: Power bar chart for center of hot spot – HIFU6, Location 2

For the HIFU6-location 3, the empirical and numerical traces become close once again (Figures: 4.1.9 to 4.1.12). The initial slopes of the traces are quite close for all three power levels. The power levels determined by the inverse method, shown in Fig. 4.1.12, are about 40% greater than the RFB values at all three power levels.

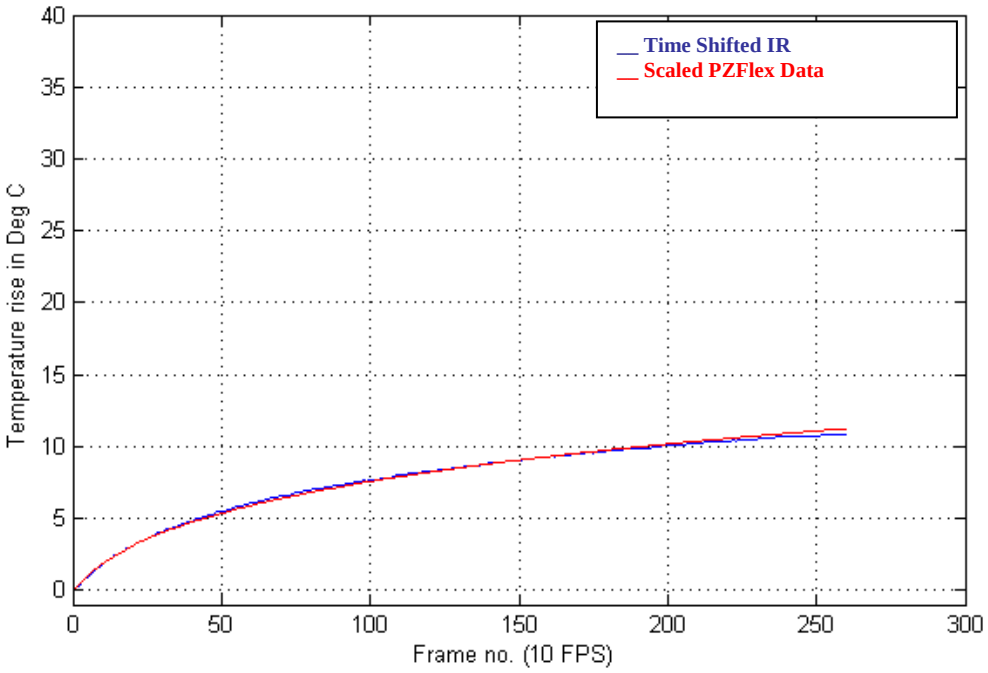

Fig. 4.1.9: Temperature trace for center of hot spot – HIFU6, Location 3, Power 3.37 W

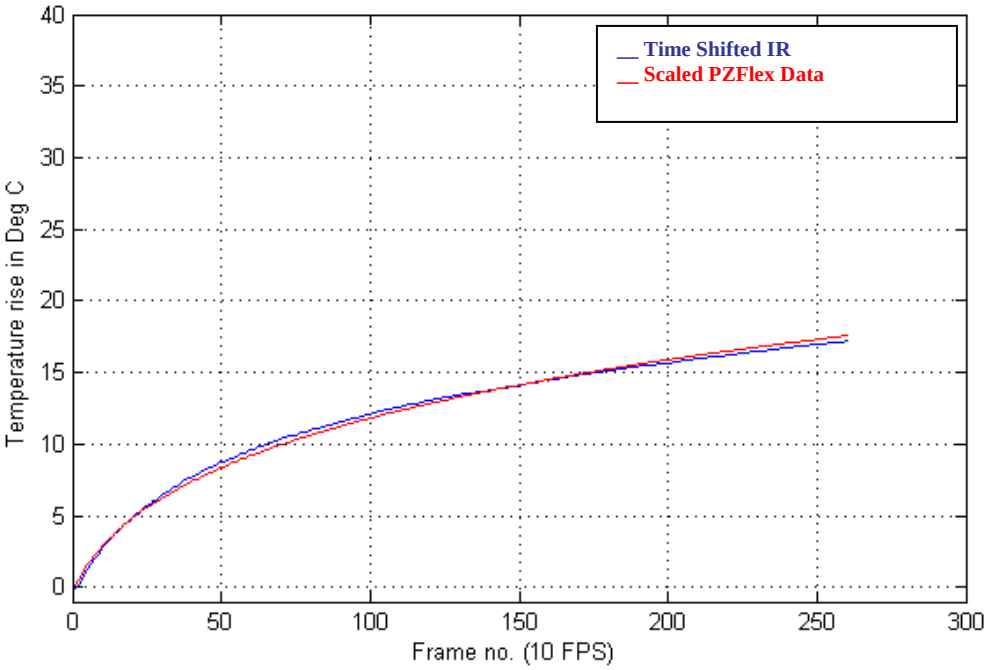

Fig. 4.1.10: Temperature trace for center of hot spot – HIFU6, Location 3, Power 5.20 W

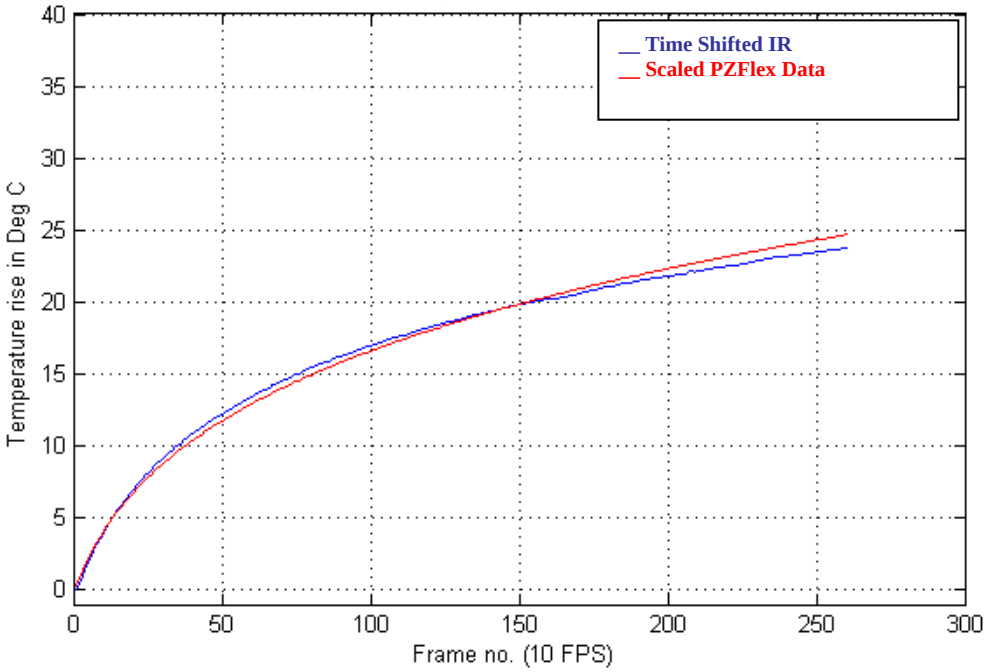

Fig. 4.1.11: Temperature trace for center of hot spot – HIFU6, Location 3, Power 7.46 W

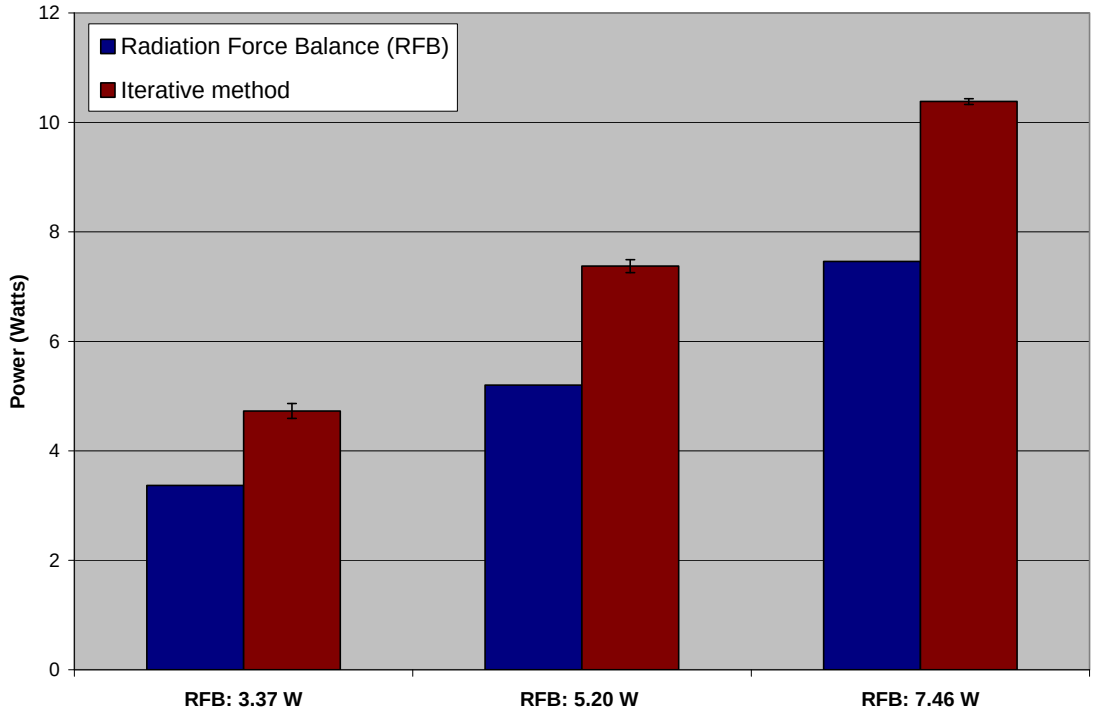

Fig. 4.1.12: Power bar chart for center of hot spot – HIFU6, Location 3

Figure 4.1.13 shows the numerical and empirical temperature traces for the case of HIFU2-location 1, at a power level of 5.37 Watts. The agreement between the two traces is not as close as compared to HIFU 6 (in Figure 4.1.1). A slight divergence can be seen for between the traces (up to 1 deg. C). For the intermediate power level of 7.71 Watts, the agreement is similar to that seen for the lowest power level (Figure 4.1.14). For the highest power of 10.48 W, the curves show similar agreement as seen in the case of previous two power levels (Figure 4.1.15). The power predicted by the inverse method is shown in Figure 4.1.16, along with radiation force balance (RFB) power measurements.

For HIFU2-location 1 (Figures 4.1.13 – 4.1.16), the power values based upon the inverse method are less than the RFB values at each power level. Also, the inverse

method predictions become less accurate with increasing power. The RFB value is about 10% above the value determined by the inverse method at the lowest power, 18% above at the intermediate power, and 22% above at the highest power.

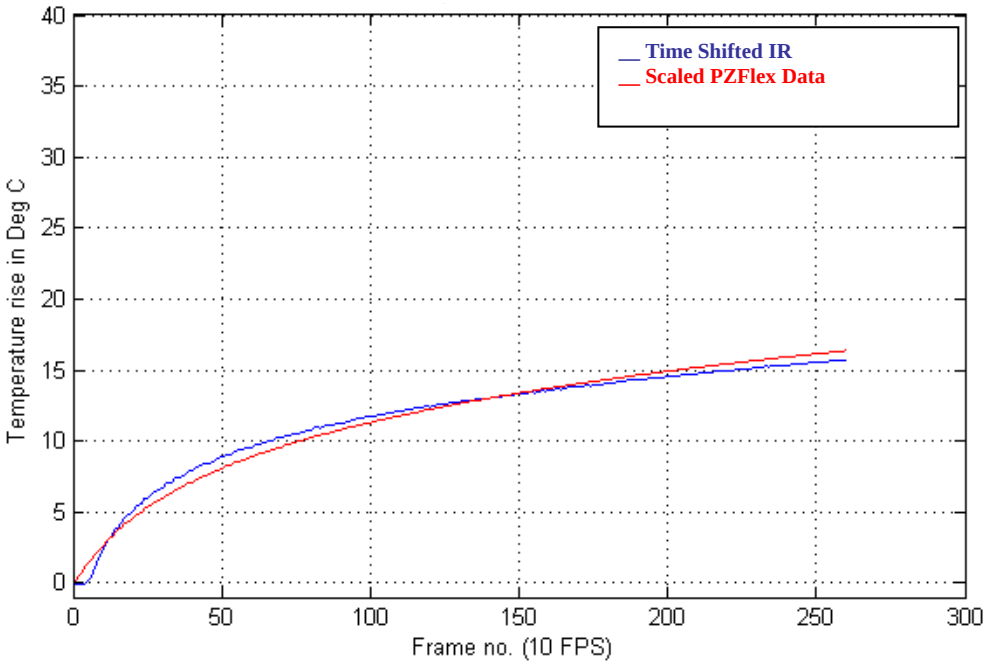

Fig. 4.1.13: Temperature trace for center of hot spot – HIFU2, Location 1, Power 5.37 W

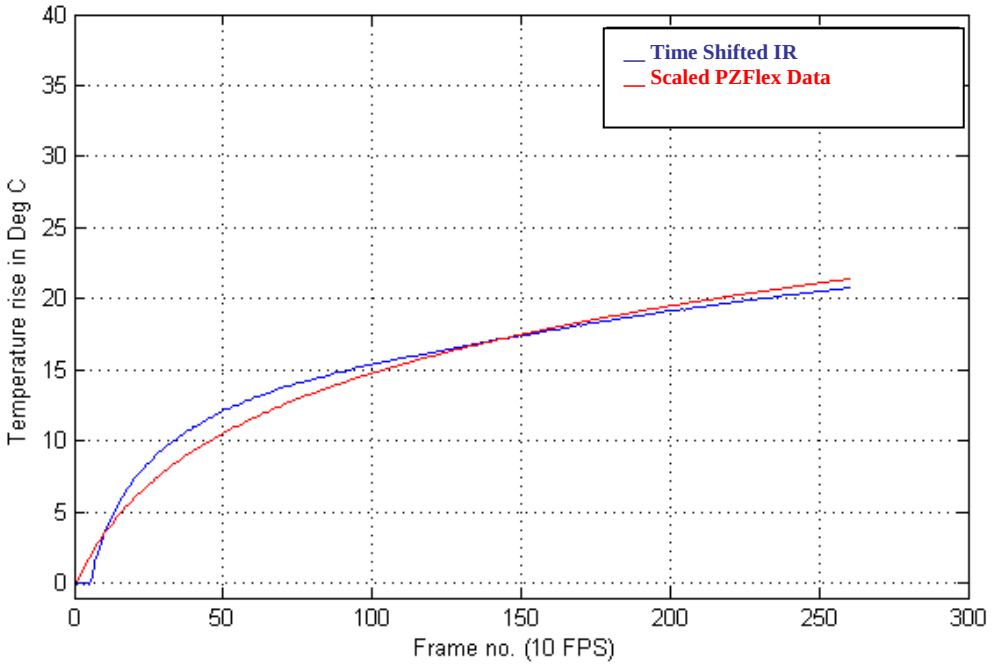

Fig. 4.1.14: Temperature trace for center of hot spot – HIFU2, Location 1, Power 7.71 W

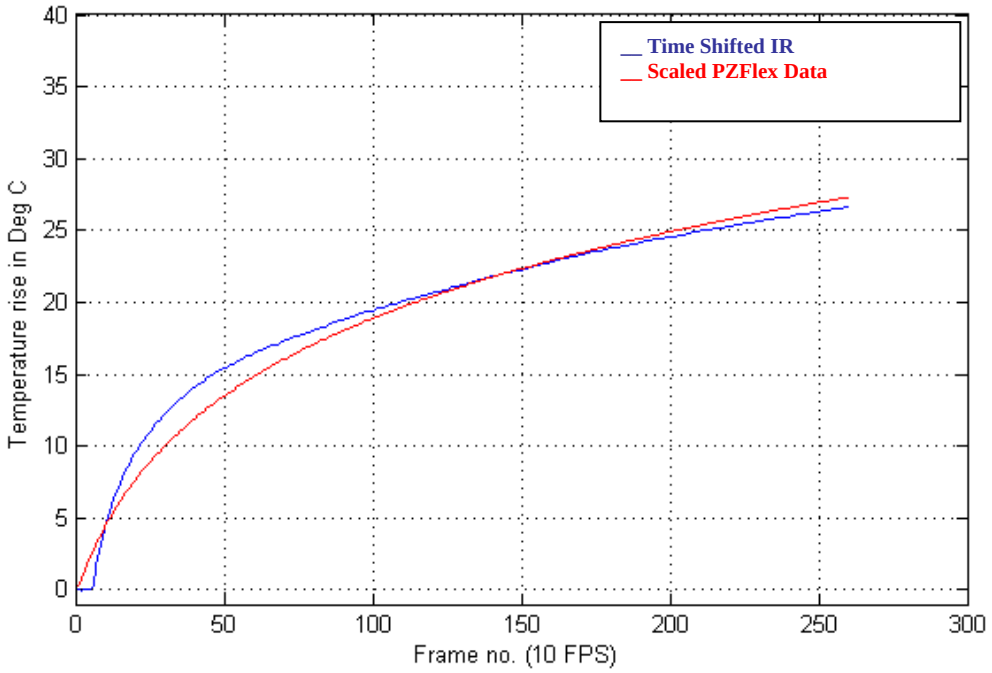

Fig. 4.1.15: Temperature trace for center of hot spot – HIFU2, Location 1, Power 10.48 W

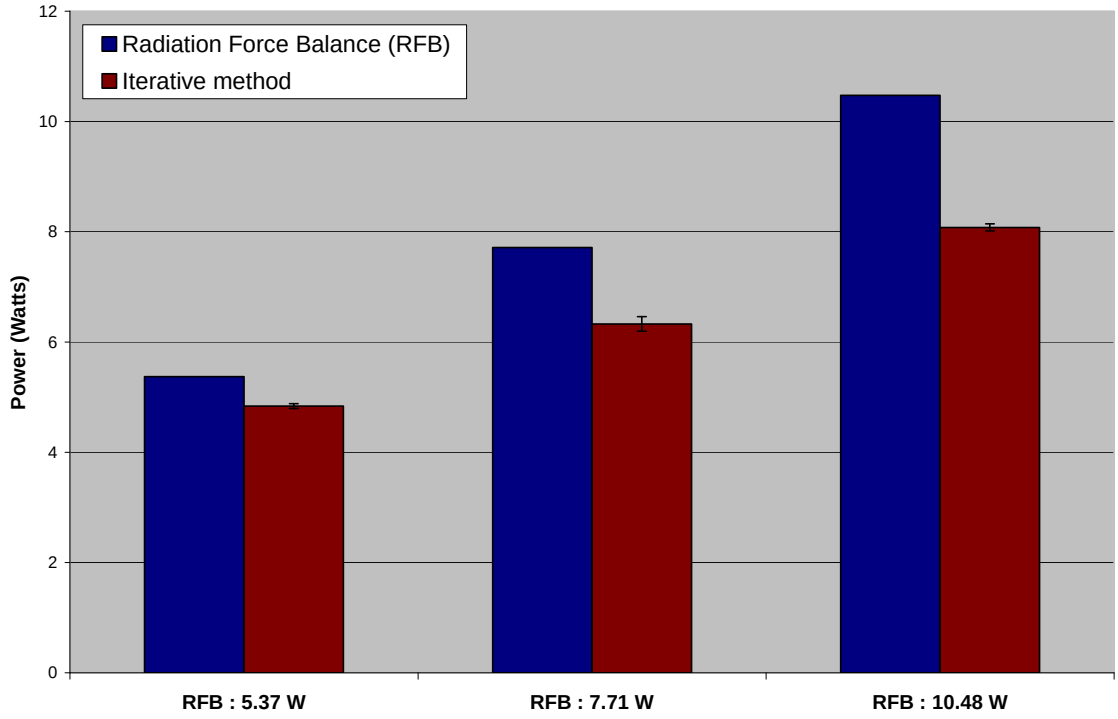

Fig. 4.1.16: Power bar chart for center of hot spot – HIFU2, Location 1

For HIFU2-location 2 (Figures 4.1.17 to 4.1.20), the agreement between the computational and empirical temperature traces is similar to that of HIFU2-location 1 (Figures 4.1.13 to 4.1.15). In each case, the initial heating rate is higher for the infrared data, but subsequent heating is not as intense as that predicted by PZFlex. The power values predicted by the inverse method, shown in Fig. 4.1.20 are closer to the infrared measurements when compared to the predictions for the previous location for HIFU2.

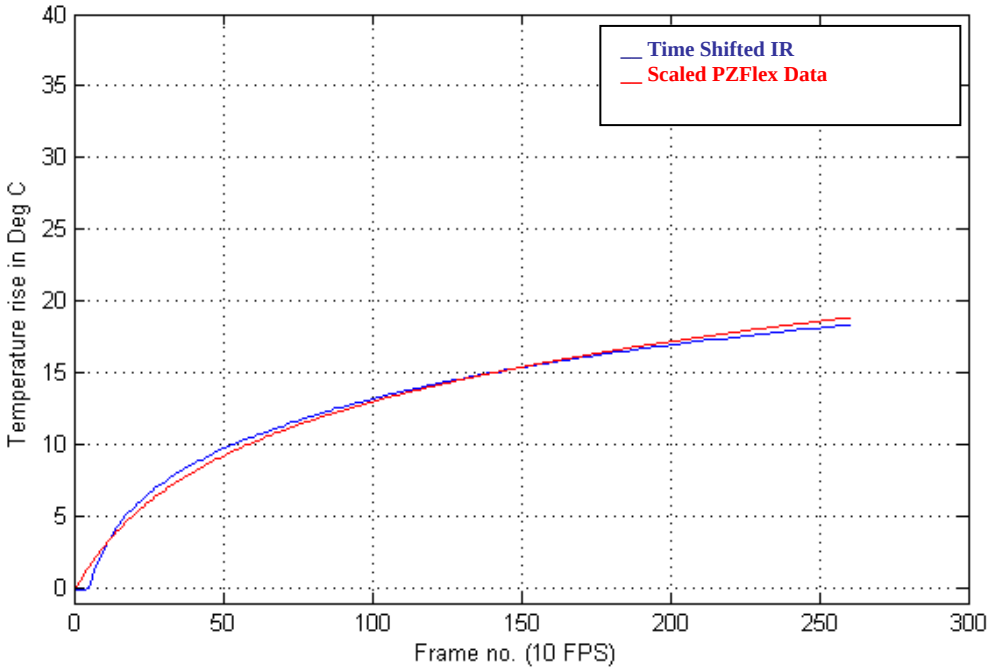

Fig. 4.1.17: Temperature trace for center of hot spot – HIFU2, Location 2, Power 5.37 W

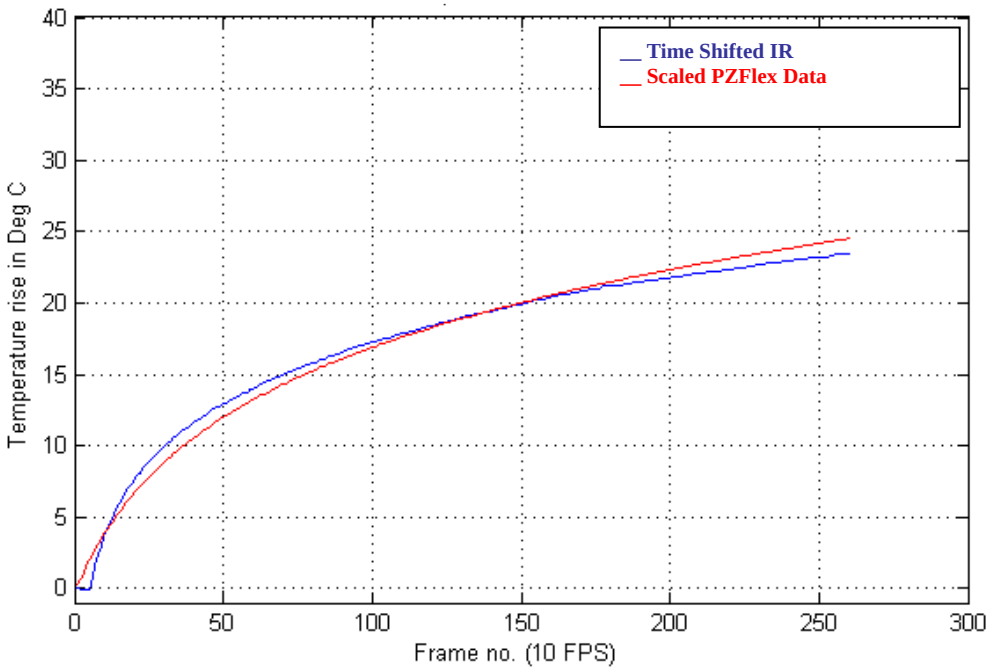

Fig. 4.1.18: Temperature trace for center of hot spot – HIFU2, Location 2, Power 7.71 W

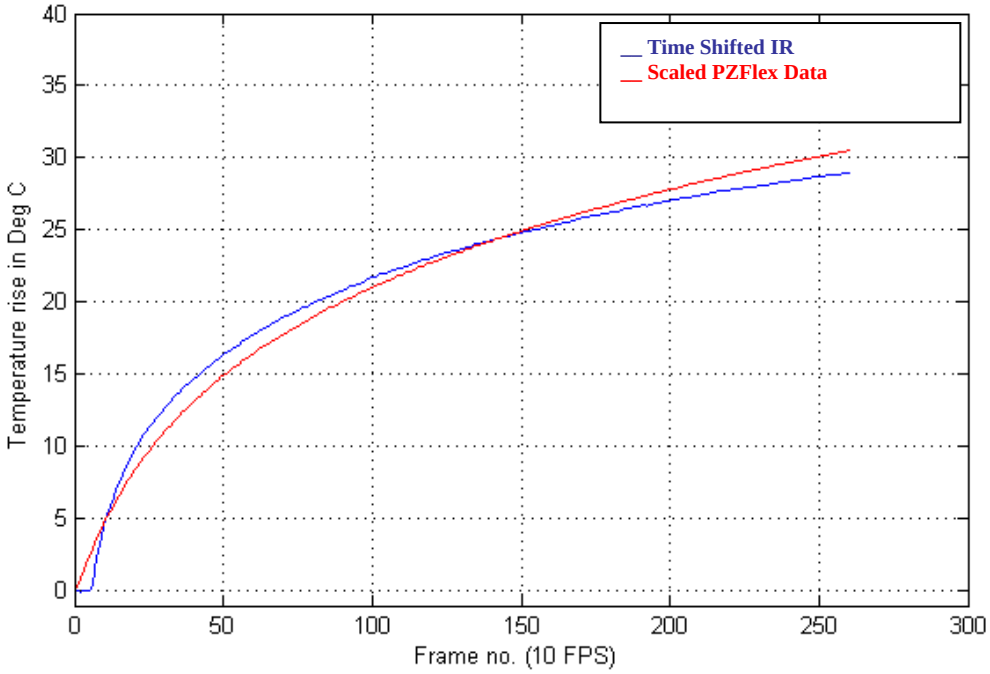

Fig. 4.1.19: Temperature trace for center of hot spot – HIFU2, Location 2, Power 10.48 W

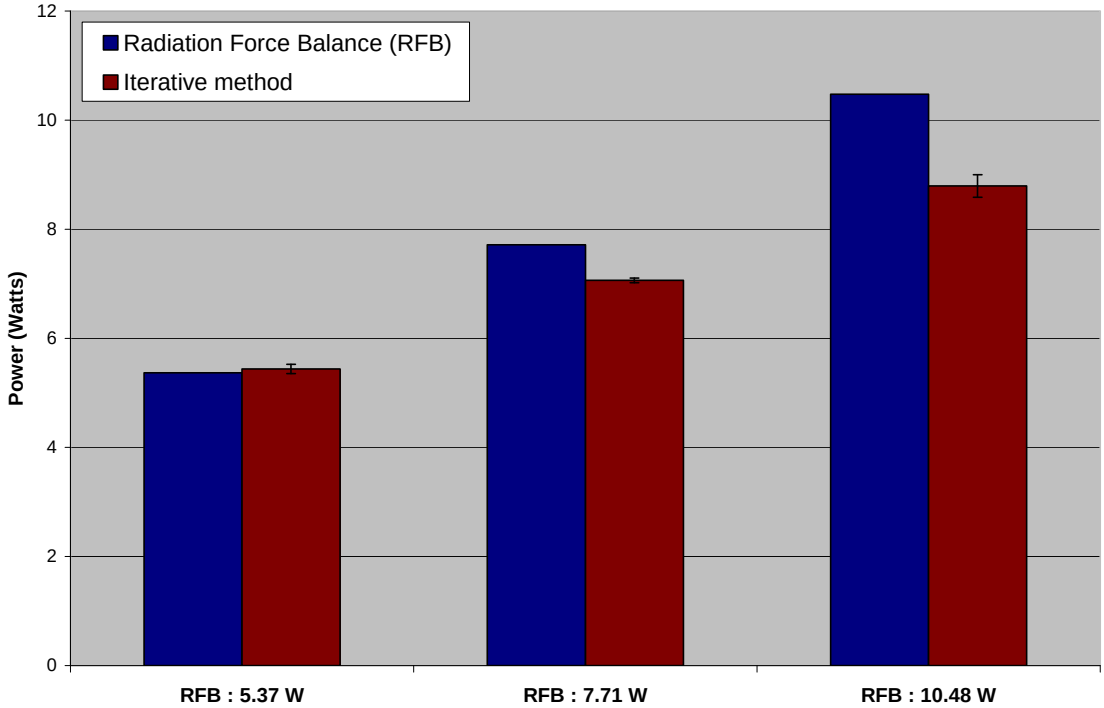

Fig. 4.1.20: Power bar chart for center of hot spot – HIFU2, Location 2

The temperature traces for HIFU2-location 3 can be seen in Figures 4.1.21 - 4.1.24, the empirical and numerical traces appear the closest when compared to the other two locations of HIFU 2. The initial slopes and the subsequent heating appear the closer for all three power levels. The power levels determined by the inverse method, shown in Figure 4.1.24, are about 19%, 12% and 8% greater than the RFB values at the lowest, intermediate and highest power levels respectively.

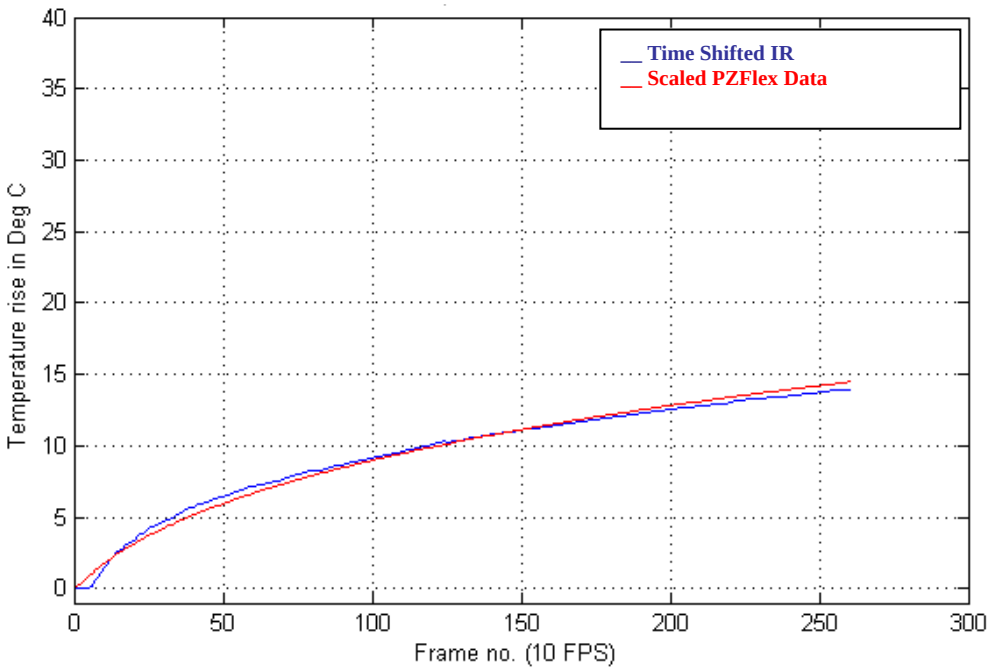

Fig. 4.1.21: Temperature trace for center of hot spot – HIFU2, Location 3, Power 5.37 W

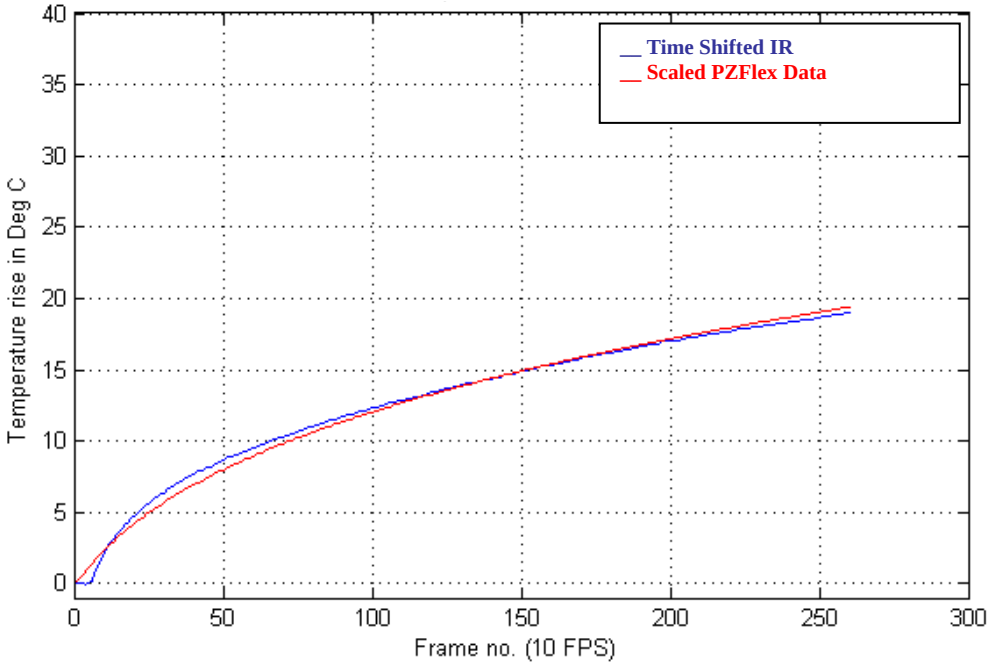

Fig. 4.1.22: Temperature trace for center of hot spot – HIFU2, Location 3, Power 7.71 W

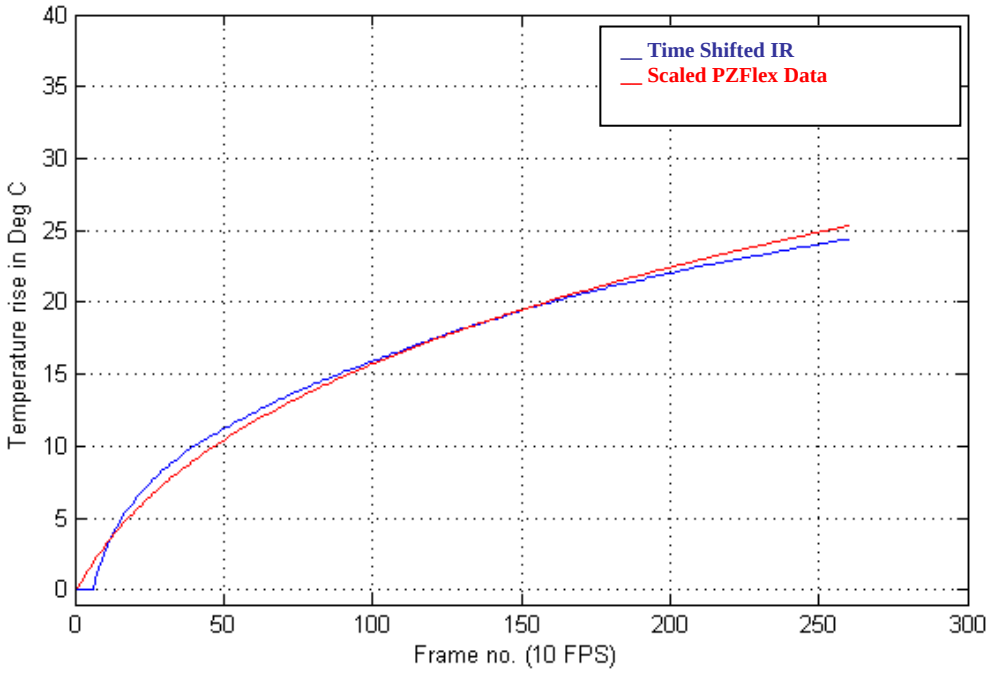

Fig. 4.1.23: Temperature trace for center of hot spot – HIFU2, Location 3, Power 10.48 W

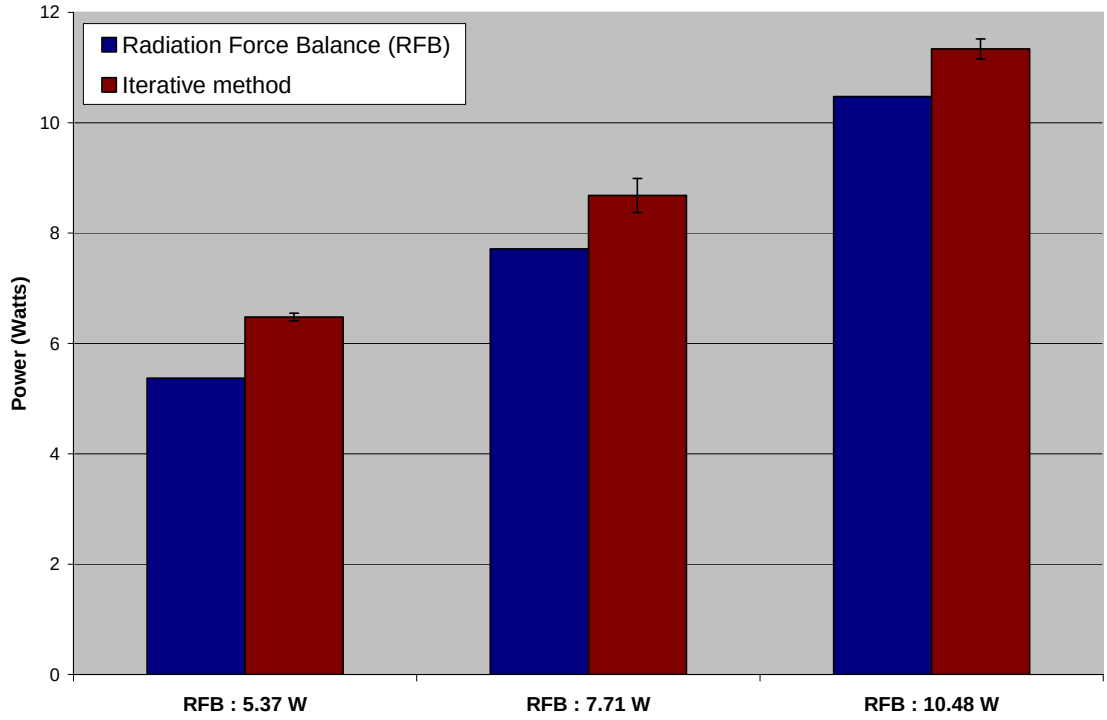

Fig. 4.1.24: Power bar chart for center of hot spot – HIFU2, Location 3

Table 4.1.1a and 4.1.1b list the difference between the RFB power values and the predicted power values for all locations and power levels, for HIFU 6 and HIFU 2 respectively.

HIFU 6	3.37 Watts RFB	5.20 Watts RFB	7.46 Watts RFB
Location 1 (9.50 cm)	25%	21%	16%
Location 2 (10.00 cm)	45%	42%	31%
Location 3 (10.50 cm)	40%	41%	39%

Table 4.1.1a

HIFU 2	3.37 Watts RFB	5.20 Watts RFB	7.46 Watts RFB
Location 1 (10.00 cm)	10%	18%	22%
Location 2 (10.75 cm)	1%	8%	16%
Location 3 (11.50 cm)	19%	12%	8%

Table 4.1.1b

Chapter 5: Summary

5.1 Summary

Several attempts were required to construct a system in which the temperature rise due to attenuation of a HIFU beam could be measured by an infrared camera, as well as simulated numerically in a reasonably straightforward way. Problems that we overcame in early designs were standing wave generation, temporal resolution of the IR camera, asymmetric heating patterns etc. In the final design, an optimization routine was employed to select the unknown transducer power and beam activation time to best fit the measured and simulated temperature fields. In some cases, the fit produced numerical and empirical curves having essentially the same shape (e.g. Figs 4.1.9, 4.1.10), providing some validation for the inverse method. In other cases, the shapes of the curves were significantly different, as in Figs. 4.1.7 and 4.1.19. The largest differences occurred with the beam focused directly upon the interface. Follow-on studies to explore these differences are described in the next section.

In terms of power predictions, the agreement between the inverse method and radiation force balance was reasonable; the average difference was around 23%. One aspect that needs to be understood is why excellent agreement between infrared and computational temperature predictions did not necessarily yield power predictions that agreed well with the radiation force value. For transducer HIFU6 at location 1, for example, the infrared and PZFlex traces essentially overlap at the lower 2 powers (Fig. 4.1.1, 4.1.2), but the power predictions agree with RFB only to within about 40%. This aspect requires further study as well.

5.2 Future work

As noted above, given the close agreement between the experimental and numerical traces for some of the exposures (e.g. Figure 4.1.1), it is somewhat surprising that the inverse method did not yield power estimates that were in better agreement with RFB values. A useful future study will be to check the simulation component of the inverse method with a plane-wave rather than focused source. A plane-wave solution to transient heating at a planar interface can be constructed following the techniques of Myers (2004), for a beam reflecting off of a bone-tissue interface.

The powers used in this study were relatively low compared to those used clinically. The maximum used in the present investigation was 10.5 Watts, while clinical power levels can exceed 100 Watts. One reason for the poor agreement between some of the inverse method and RFB power values could be the lower accuracy of the infrared camera at low temperatures. It is also possible that at the low end of the power range, RFB measurements are less accurate than the 10% value quoted by Maruvada et al. (2007).

Application of the inverse method at higher powers is an important area of future research. Part of the original motivation for using lower powers was the desire to avoid boiling the tissue-mimicking material during the 30-second exposures. Boiling of the tissue-mimicking material occurs around 100 deg. C in the phantom as in real tissues. For a base (room) temperature of slightly less than 30 degrees, a 70-degree temperature rise should be possible. Assuming the temperature rise is roughly proportional to power, the power can be increased about a factor of 3 since presently maximum temperature increases are around 25 degrees. Another important change would be to increase the

power and decrease the exposure time. Exposure times of even a few seconds could be used, to investigate power levels on the order of 100 Watts.

The inverse method developed thus far has used infrared temperature measurements at a single spatial location - the center of the hot spot - in order to compare with computational values. The infrared system records temperatures across the entire TMM/air interface. The inverse method will be extended to include locations other than the hot spot in the optimization process.

The output of the iterative method as described in this thesis is an estimate of the total radiated acoustic power. A more valuable quantity than total power is the radial distribution of intensity. The method will be extended to compute intensity distribution in the following manner. We are interested in the first one or two seconds of activation, where radial conduction of heat is negligible. This is the portion of the Temperature vs. time curve where the temperature increase is linear, roughly one second in duration. When conduction is ignored, the heat equation (Eq. 3.3) reduces to

$$\rho c_p \frac{\partial T}{\partial t} = 2\alpha I(z,r), \qquad \text{Equation 5.1}$$

the solution to which is

$$T = \frac{2\alpha I}{\rho c_p} t\,. \qquad \text{Equation 5.2}$$

Solving for the intensity yields

$$I(r,z) = \frac{\rho c_p T(r,z,t)}{2\alpha t}. \qquad \text{Equation 5.3}$$

The intensity will be computed in this manner for a sequence of time values. For a short period of time, prior to conduction becoming important, the intensity estimate should be independent of time.

Another extension of the present work that has important practical impact is to determine the intensity distribution in the absence of the air interface. In clinical applications of HIFU, the air interface will not be present, and it is useful to relate the intensity measured by IR and the physiological situation. With the air interface present, the total acoustic intensity consists of a term due the incident beam, another for the beam reflected off of the interface, and an interference field. It is likely that the interference field, which varies rapidly in space, can be ignored under some circumstances. These circumstances will be established, by first studying plane wave field. Extensions to beams will then be made using PZFlex.

5.3 Conclusion

The inverse method based upon infrared thermometry shows promise as a tool for quantitatively measuring radiated power and intensity distributions for HIFU beams. While infrared imaging has been used previously in order to measure temperature in HIFU phantoms (Shaw A, Journal of Physics Conference Series I 2004) or to compare one transducer to another in terms of power or intensity, it has not been used to quantitatively predict power or intensity distributions for a single transducer. Quantitative predictions of intensity (or pressure, derived from intensity) are important for predicting potential thermal or cavitation damage (Rabkin et al. 2005) as well as for verifying transducer designs. Being noninvasive, the technique does not suffer from

thermocouple artifacts or other problems involving sensors interacting with the HIFU beam. The technique does require repeated solutions of the sound propagation equation, especially at higher powers where the sound field for one level of transducer pressure is nonlinearly related to the sound field at another transducer pressure. Still, power determinations for new transducers can be performed with overnight runs on a personal computer (much faster on network clusters). The next important step in transducer characterization is the determination of acoustic intensity fields along side the power determinations.

REFERENCES

Christensen D, “Ultrasonic Biointsrumentation”, Wiley, 1988

CRADA (Cooperative Research and Development Agreement): Epicor Medical and FDA, March 2007

Hansen L, NIST Emissivity Laboratory, March 2009

Hariharan P, Myers MR, Robinson RA, Maruvada SH, Sliwa J, and Banerjee RK, “Characterization Of High Intensity Focused Ultrasound Transducers Using Acoustic Streaming”, J. Acoust. Soc. Am. 123 (3):1706-1719, March 2008

Hariharan P, “Free Field Characterization Of High Intensity Focused Ultrasound (HIFU) Transducers Using Acoustic Streaming”, PhD dissertation, University of Cincinnati, 2008

Harland AR, Petzing JN, and Tyrer JR. “Non-invasive measurements of underwater pressure fields using laser Doppler Velocimetry”, Journal of Sound and Vibration 2002; 252(1): 169-177

Infrared Thermography Field Application Guide, EPRI, Palo Alto, CA: 1999. Report TR-107142

King RL, Herman BA, Maruvada SH, Wear KA, Harris GR, “Development of a HIFU Phantom”, Proceedings for International Society on Therapeutic Ultrasound 2006, Oxford, UK, 2006

Liu Y, Kon T, Chuanyuan L, and Zhong P, “High Intensity Focused Ultrasound-Induced Gene Activation in Solid Tumors”, J. Acoust. Soc. Am, vol 120, pp 492-501

Maruvada S, Harris GR, Herman BA, and King RL, “Acoustic Power Calibration Of High-Intensity Focused Ultrasound Transducers Using A Radiation Force Technique”, J.Acoust. Soc. Am. 2007, 121(3): 1434-1439

Michel JM, “Introduction To Cavitation And Super Cavitation”, Labaratoire des Ecoulements Geophysiques et Industriels BP 53 -38041, France, 2001

Morris P, Hurrell A, Shaw A, Zhang E, Beard P. “A Fabry-Perot Fiber-Optic Ultrasonic Hydrophone For The Simultaneous Measurement Of Temperature And Acoustic Pressure”, J. Acoust. Soc. Am. Volume 125, Issue 6, pp. 3611-3622 (June 2009)

Myers MR, “Transient Temperature Rise Due To Ultrasound Absorption At A Bone/Soft-Tissue Interface”, Journal of the Acoustical Society of America, Vol. 115, No. 6, pp. 2887-2891, June 2004

Rabkin BA, Zderic V, Vaezy S, “Hyperecho In Ultrasound Images Of HIFU Therapy:Involvement Of Cavitation”, Ultrasound in Medicine & Biology, Volume 31, Issue 7, July 2005, Pages 947-956

Shaw A, “Advanced Metrology for Ultrasound in Medicine”, Journal of Physics Conference Series I, Institute of Physics Publishing, 2004

Shaw A and ter Haar GR. “Requirements For Measurement Standards In High Intensity Focused (HIFU) Ultrasound Fields”, National Physical Laboratory (NPL) report 2006; ISSN 1744-0599

Szabo T, “Diagnostic Ultrasound Imaging: Inside out”, Academic press, 2004

ter Haar GR, Acoustic surgery. Physics Today 2001; 54(12):29-34

Theobald P, Thompson A, Robinson S, Preston R, Lepper P, Swift C, Yuebing W, and Tyrer J, “Fundamental Standards For Acoustics Based On Optical Methods – Phase Three Report

For Sound In Water", National Physical Laboratory (NPL) report 2004; CAIR9 ISSN 1740-0953

Zderic V, Keshavarzi A, Noble ML, Paun M, Sharar SR, Crum LA, Martin RW, Vaezy S. "Hemorrhage Control in Arteries Using High-Intensity Focused Ultrasound: A Survival Study", Ultrasonics 2006;44:46-53

Zhai, L., Yufeng Zhou, and Pei Zhong, "Dosimetry Measurement Of HIFU Field Using A Fiber Optical Probe Hydrophone", J. Acoust. Soc. Am. Volume 115, Issue 5, pp. 2491-2491 (May 2004)

Appendix A

The first PZFlex file contains the model, transducer dimensions and properties. This file is used to simulate wave propagation through the medium and compute the energy loss over one cycle. This energy loss information is then used by the heating file to compute the temperature rise due to the acoustic field due to the transducer and the TAS value. The files shown below are the wave propagation file and the heating file for HIFU6 with a TAS value of 10.5 cm (Location 3).

1. PZFlex Wave propagation file

```
mem 10000

rest no

titl Focused Wave Propagation
c
c Materials:
c   water is modeled as linear, elastic
c   TMM is modeled as nonlinear, viscoelastic ("tisu" material model & "sdmp" damping model)
c   air is modeled as linear, elastic
c Simulation:
c   Run until steady-state is achieved and/or wave has propagated to other side of model
c   then capture LOSS over one cycle
c
c ******************************** ALL UNITS IN MKS ****************************

symb #get { labl } jobname

c
c ********************************** USER INPUT ********************************
c
symb xdcr = focused          /* if you wish to model a focused transducer set $xdcr = "focused";
                             /* any other name (such as "plane") will model a planar transducer;
                             /* be careful to properly spell "focused", or else it will default to planar.
symb graph = yes             /* if you wish to have PZFlex make graphs/plots during the run, then set the
                             /* parameter $graph equal to "yes"; otherwise, it will not make graphs/plots.
symb power = 5.5             /* this is the acoustic power level of the transducer (unit of Watts)
symb rho_watr = 998.2        /* these properties for water are used, below, to calculate the ...
symb sspd_watr = 1482.0      /* initial pressure, "p0", at the face of the transducer.
                             /* these properties for water come from ICRU Report #61

symb ipmax_prev = 1          /* enter the nodal location of maximum positive pressure
c                            as determined from a previous simulation and stored
```

```
c                          as $ipmax.
c
c ******************************** Model Definition ***************************
c
c Model sizes - these are the thicknesses of each layer of material in the model (in meters)
c
symb watrlayr = 6.50e-2
symb tmmlayr = 4.00e-2

symb airlayr = 3.00e-2
c
c Model sizes - radial dimensions
c
symb tmmrad = 6.0e-2      /* radius of model
symb xdcrrad = 5.0e-2     /* radius of transducer is equal to that of domain
c
c Focal parameters
c
symb nfoc = 40          /* number of sections to focus pressure from
symb focdist = 10.0e-2   /* depth of focus
symb velfoc = ( ( 10.00e-2 ) / ( ( $watrlayr / 1482 ) + ( ( 10.00e-2 - $watrlayr ) / 1250 ) ) )
c symb velfoc = $sspd_watr  /* assumed velocity to calculate focal delays


c
c Find element size needed
c
symb freq1 = 1.155e6       /* set this to the highest frequency that will exist - consider nonlinearity
symb velmin = 1500.       /* set this to the lowest wavespeed (i.e., that in the water layer)
symb numelem = 80         /* along propagation path, set >>15 for accuracy
symb #print on
symb wavemin = $velmin / $freq1    /* this is the smallest wavelength that will be adequately ...
symb box = $wavemin / $numelem     /* modeled in this simulation

symb x1 = 0.0
symb x2 = $x1 + $watrlayr
symb x3 = $x2 + $tmmlayr
symb x4 = $x3 + $airlayr
symb xmax = $x4
symb x2mid = ( $x3 + $x2 ) / 2.         /* mid-point in TMM


symb y1 = 0.0
symb y2 = $y1 + $xdcrrad
symb y3 = $y1 + $tmmrad
symb ymax = $y3

symb i1 = 1
symb i2 = $i1 + nint ( ( $x2 - $x1 ) / $box )
symb i3 = $i2 + nint ( ( $x3 - $x2 ) / $box )
symb i4 = $i3 + nint ( ( $x4 - $x3 ) / $box )

symb indgrd = $i4                                  /* node at end of domain

symb j1 = 1
symb j2b = $j1 + nint ( ( $y2 - $y1 ) / $box )
```

```
c
c Ensure even element spacing for focussing elements
c
symb jwide = nint ( ( $j2b - $j1 ) / $nfoc )
symb j2 = $j1 + ( $nfoc * $jwide )
symb j3 = $j2 + nint ( ( $y3 - $y2 ) / $box )
symb jndgrd = $j3
symb boxt = ( $box * 10. )
symb #print none



grid $indgrd $jndgrd axix     /* axisymmetric model

geom
   xcrd $x1 $x2 $i1 $i2
   xcrd $x2 $x3 $i2 $i3
   xcrd $x3 $x4 $i3 $i4
   ycrd $y1 $y2 $j1 $j2
   ycrd $y2 $y3 $j2 $j3
   end

c Use zones to increase computational speed.
zone * $i1    $i3-1    $j1  $jndgrd
zone * $i3-1  $indgrd    $j1  $jndgrd
c c zone * $i4+1  $indgrd  $j1  $jndgrd

matr
c
c    Mechanical properties
c
    wvsp on   /* this param allows specification of waves speeds in lieu of stiffness moduli

c    The material "type" for the water is the default of "linear elastic".
c    (material name, density, bulk wave spd, shear wave spd)

    prop watr $rho_watr $sspd_watr 0. 0.
    prop air   1.2  343. 0. 0.                    /* data for air per the web

    vdmp watr 1.0e6   db 0.0022 0.0 1.000e6 0.0 0.01   /* data per ICRU Report #61; 0.0022 dB/cm
    vdmp air 1.100e6  db 1.94   0.0 1.100e6 0.0 0.01   /* data for air per the web

c    NOTE: The "vdmp" model can only be used with "elastic materials; if the TMM is defined as a
c    If the material "type" for the TMM is "tissue" it allows specifying a nonlinear, B/A, material.
c    Note that the damping model that may be used when the TMM is treated as "elasitic" can NOT
c    be used when it is treated as a "tissue" - a new damping model must be used, as described below.
c    Also note that along with the use of this "nonlinear" material, the output pressure parameter must
c    specify "apres" within the "pout" specification for "pres" (which is a linear parameter when "apres"
c    is not specified) so that the code knows to track nonlinear pressure behavior).
c           prop tmm  1000.0 1561. 0. 0.                    /* previous "elastic" tissue model
c       vdmp tmm  1.105e6 db 0.588  0.0 1.105e6 0.0 0.01   /* previous damping model
c
    type tisu
    wvsp on
    symb alpha = 1.9
```

```
    symb exp = 1.25
    symb pmax = 20.e6
    symb pmaxn = -20.e6
    prop tmm  1107.0 1250.0 0.01 0.0 0.0            /* rho measured by Nell; sspd by Dr. Liu
    8.00 $pmaxn $pmax                               /* B/A; pmax, pmin
    sdmp tmm $freq1 db $alpha 0.0 $freq1 $exp 0.01     /* use the "sdmp" damping model for "tisu"
materials
                                        /* attenuation: $alpha*f^$exp dB/cm-MHz
c    Thermal properties (specific heat [J/kg-degC], thermal conductivity [W/m-degC])
c
    thrm watr  4182. 0.60     /* data per ICRU Report #61 (diffusivity = 0.144 mm^2/s)
    thrm tmm   3876. 0.693    /* data measured on 12/19,22,31/08 (diffusivity = 0.16 mm^2/s)
c    thrm tmm   3867. 0.58     /* data per R. King et al. (2007) (diffusivity = 0.15 mm^2/s)

    thrm air   1005. 0.0257   /* data for air per the web
                        /* (diffusivity = 21.3 mm^2/s or ~ 150 times that of water & tmm)

    end

site
    regn watr
    regn tmm   $i2 $i3 $j1 $j3

    regn air   $i3 $i4 $j1 $j3
    end

boun
    side xmax absr         /* absorbing boundary condition at distal end of domain
    side ymin symm          /* symmetric boundary condition along central axis
    side ymax absr         /* absorbing boundary condition at outer radius of domain
    end
c
c ******************************** Solution Parameters ****************************
c
c Define the transducer output:
c "p0" is the peak pressure at the face of the transducer.  It presumes the following:
c >  a uniform distribution over the face of the transducer;
c >  the transducer is submerged in water (hence properties for water are used to calculate "p0";
c >  p0 is in units of Pascals.
c
symb p0 = sqrt ( ( 2 * $rho_watr * $sspd_watr * $power ) / ( 3.141592 * $xdcrrad ** 2 ) )
func sine $freq1 $p0 0.0 0.0 0.0 5        /* apply a CONTINUOUS sine load and slowly ramp it over 5
cycles;
c                                  the ramping is done to reduce transients in the solution;
c                                  for one (1.) period, only, set the second 0.0 to "1."

c
c Computational window for efficiency
c
wndo 1 2 1 $jndgrd

c
c Pressure loads
c
plod
    vctr down 1. 0. 0.
```

```
c
c Work out time shifts for each pressure source
c
symb #print on
symb jstart = $j1
symb jstop = $jstart + $jwide
do loopi I 1 $nfoc

  symb #get { xpos1 ypos1 } crdnode 1 $jstart 1
  symb #get { xpos2 ypos2 } crdnode 1 $jstop 1
  symb ymid$I = ( $ypos2 + $ypos1 ) / 2.
  symb jmid$I = nint ( ( $jstart + $jstop ) / 2. )
  symb dist$I = ( ( $ymid$I ** 2. ) + ( $focdist ** 2. ) ) ** 0.5
  symb time$I = $dist$I / $velfoc

  symb jstart = $jstop
  symb jstop = $jstart + $jwide
  symb #print none
end$ loopi
symb #print on
c
c Now apply - shift times so edge fires at t=0.
c
        symb jstart = $j1
        symb jstop = $jstart + $jwide
do loopi I 1 $nfoc

        symb timeshft = $time$I - $time$nfoc
        symb time$I
        symb time$nfoc
        symb #print none

if ( $xdcr eq focused ) then
   pdef p$I func 1.0 -$timeshft     /* negative timeshift means 'forward' in time
else
   pdef p$I func 1.0
endif
   sdef p$I down $i1 $i1 $jstart $jstop
   symb #print on
   symb jstart = $jstop
   symb jstop = $jstart + $jwide
end$ loopi

   end
symb #print none
c
c Get pressure shapes at main frequency as well as 2nd and 3rd harmonics - in highly nonlinear
c problems, may want to save even higher harmonics.
c
symb freq2 = 2. * $freq1
symb freq3 = 3. * $freq1
shap
        data pres
        freq $freq1   /* 1st harmonic (fundamental)
        freq $freq2   /* 2nd harmonic
        freq $freq3   /* 3rd harmonic
```

```
        end

c NOTE: "calc" must precede "pout" or not all data will be properly calculated and saved!
c       Also note that "apres" is used to output rarefactional pressures as negative values
c       and compressive pressures as positive (standard convention in acoustics)
calc
        disp
        loss
        pres apres          /* allows pressure contour plot during post-processing
        max pres pmin pmax   /* calculate max and min pressures during simulation
        velm              /* allows velocity contour plot during post-processing
        end

c The following writes-out time-history data to the file "sonication.flxhst."
c The file "sonication.revinp" is then used to post-process (plot & write text files)
c those time histories.
c Note that the following line defines the node number ($ifocus) that is closest to the
c focus.  It seems that the $ifocus parameter value is not saved properly and/or recalled
c properly in the symb.sonication file, for some unknown reason.  So, this exact same line
c must also appear within the heating.flxinp file in order to properly record temperatures
c at the focus!

symb #print on
symb #get { ifocus jfocus kfocus } clsnode $focdist 0.0 0.0
symb #get { i2mid jj kk rdist } clsnode $x2mid 1 1  /* node corresponding to mid-point of TMM
symb #print none


pout

        hist func                       /* store input pressure history (record #1)
        hist pres 2 2 1  1 1 1              /* store press just in front of xdcr face (record #2)
        hist xvel 2 2 1  1 1 1              /* store xvel just in front of xdcr face (record #3)
        hist pres $i2 $i2 1 $j1 $j1 1         /* store pressure at front face of TMM (record #4)
        hist pres $i2mid $i2mid 1 $j1 $j1 1     /* store pressure at mid-point of TMM (record #5)
        hist pres $ifocus-1 $ifocus-1 1 $j1 $j1 1   /* store the pressure at focus (record #8)
        end

prcs

if ( $graph eq yes ) then
c Display the model prior to execution of the solution
grph
    mirr y
    line no
    nvew 1
    colr tabl matr 5
    map watr 18
    map tmm 10
    map air 26
    plot matr


    draw node $i2 $i2 $j1 $jndgrd
    draw node $i3 $i3 $j1 $jndgrd
    draw node $i4 $i4 $j1 $jndgrd
```

```
    end
endif
c
c ******************************** Solution Execution ******************************
c
c Run until steady-state is achieved; i.e., until the pressure wave has exited the model.
c Thus, "turn on" the transducer for a total of $maxn cycles, where the variable $maxn
c is the number of cycles it takes for the smallest wavelength ($wavemin) to traverse
c the maximum travel distance within the model ($distmax).

c The following calculation is VERY important and, if done incorrectly, will yield inaccurate results.
c The following calculates the propagation distance that will be traveled - that distance
c is then used to determine the necessary number of $maxn cycles.
if ( $xdcr eq focused ) then
        symb distmax = sqrt ( $xdcrrad ** 2 + $focdist ** 2 ) + ( $xmax - $focdist )
else
        symb distmax = $xmax
endif

c If there are internal reflections, run it longer by multiplying $maxn by some factor other than "1":
symb maxn = 1.9 * nint ( $distmax / $wavemin )     /* this new simulation allows waves to return to xmin
and possibly
                                        /* reflect back and forth a bit to see if any thermal effects from such
reflections
do loop n 1 $maxn
set pmax 0.0          /* This re-sets the values of pmax and pmin so that any transient effects are not
captured
set pmin 0.0          /* in their values when the steady-state solution is executed below ("exec cycl 1").
exec cycl 1           /* This actually executes (i.e., runs) the analysis - it runs ONE cycle per loop.

c grph              /* IMPORTANT NOTE REGARDING MOVIES (avi files):
c           set imag avi  /* This command sets the image mode to "avi" so that the propagation of the pressure
c           end           /* vave (in the following do loop) can be replayed as a movie.  But, do this only once
                    /* (i.e., outside of the do loop, and do not use "set imag tiff" anywhere else in this file
                    /* because the two formats are not compatible and can not be switched back and forth!
if ( $graph eq yes ) then
grph
        plot pres     /* this plots the pressure front as it propagates

        end
endif

end$ loop

c The following 2 lines are specific to CONTINUOUS wave simulations:
c Set loss array to zero, run for 1 cycle to accumulate loss/cycle.
c This is used in a subsequent heating analysis.
c
set loss 0.           /* zero loss array
exec cycl 1           /* Run the simulation for one additional cycle and save the state for subsequent heating
analysis

c Write out loss array for entire run to file, along with other info of interest
data
    file out $labl.loss
```

```
    out modl
    out loss
    out pres
    out pmin
    out pmax
    end


symb #get { endtime } timenow
symb #msg 1
End simulation time = $endtime

symb #save symb.$labl

stop
```

2. PZFlex Heating file

```
mem 1000

rest no

titl Focused Wave Propagation
c
c ******************************** ALL UNITS IN MKS ****************************

c
c ******************************** USER INPUT ****************************
c
symb graph = yes              /* if you wish to have PZFlex make graphs/plots during the run, then set the
                        /* parameter $graph equal to "yes"; otherwise, it will not make graphs/plots.
symb #read symb.sonication
symb tstep = 0.10             /* enter the time-step to be used for this simulation
symb sonication_time = 30.0     /* enter total sonication time for this simulation
symb prf = 100.e3             /* enter the pulse repetition frequency

c
c ******************************** Model Definition ****************************
c
c Model sizes - these are the thicknesses of each layer of material in the model (in meters)
c
symb watrlayr = 6.50e-2
symb tmmlayr = 4.00e-2
symb airlayr = 3.00e-2

c
c Model sizes - radial dimensions
c
symb tmmrad = 6.0e-2      /* radius of tissue model
symb xdcrrad = 5.0e-2     /* radius of transducer is equal to that of domain

c
c Focal parameters
c
symb nfoc = 40           /* number of sections to focus pressure from
symb focdist = 10.0e-2   /* depth of focus
symb velfoc = ( ( $watrlayr + $tmmlayr ) / ( ( $watrlayr / 1482 ) + ( $tmmlayr / 1250 ) ) )

c Find element size needed
c
symb #print on
symb freq1 = 1.155e6       /* set this to the highest frequency that will exist - consider nonlinearity
symb velmin = 1500.       /* set this to the lowest wavespeed (i.e., that in the water layer)
symb numelemh = 5         /* along propagation path, set >>15 for accuracy
symb wavemin = $velmin / $freq1    /* this is the smallest wavelength that will be adequately ...
symb box = $wavemin / $numelemh    /* modeled in this simulation

symb x1 = 0.0
symb x2 = $x1 + $watrlayr
symb x3 = $x2 + $tmmlayr
symb x4 = $x3 + $airlayr
```

```
c c symb x5 = $x4 + $airlayr
symb xmax = $x4
c symb xcarcmid = ( $x4 + $x3 ) / 2.    /* mid-target in x

symb y1 = 0.0
symb y2 = $y1 + $xdcrrad
symb y3 = $y1 + $tmmrad
symb ymax = $y3

symb i1 = 1
symb i2 = $i1 + nint ( ( $x2 - $x1 ) / $box )
symb i3 = $i2 + nint ( ( $x3 - $x2 ) / $box )
symb i4 = $i3 + nint ( ( $x4 - $x3 ) / $box )


symb indgrd = $i4                                   /* node at end of domain

symb j1 = 1
symb j2b = $j1 + nint ( ( $y2 - $y1 ) / $box )


c
c Ensure even element spacing for focussing elements
c
symb jwide = nint ( ( $j2b - $j1 ) / $nfoc )
symb j2 = $j1 + ( $nfoc * $jwide )
symb j3 = $j2 + nint ( ( $y3 - $y2 ) / $box )
symb jndgrd = $j3
symb #print none
grid $indgrd $jndgrd axix     /* axisymmetric model

geom
   xcrd $x1 $x2 $i1 $i2
   xcrd $x2 $x3 $i2 $i3
   xcrd $x3 $x4 $i3 $i4
   ycrd $y1 $y2 $j1 $j2
   ycrd $y2 $y3 $j2 $j3
   end

matr
c
c   Mechanical properties
c
    wvsp on   /* this param allows specification of waves speeds in lieu of stiffness moduli

c   The material "type" for the water is the default of "linear elastic".
c   (material name, density, bulk wave spd, shear wave spd)

    prop watr $rho_watr $sspd_watr 0. 0.
    prop air   1.2  343. 0. 0.                    /* data for air per the web

    vdmp watr 1.0e6   db 0.0022 0.0 1.000e6 0.0 0.01   /* data per ICRU Report #61; 0.0022 dB/cm
    vdmp air 1.100e6  db 1.94   0.0 1.100e6 0.0 0.01   /* data for air per the web

c   NOTE: The "vdmp" model can only be used with "elastic materials; if the TMM is defined as a
c   If the material "type" for the TMM is "tissue" it allows specifying a nonlinear, B/A, material.
```

```
c    Note that the damping model that may be used when the TMM is treated as "elasitic" can NOT
c    be used when it is treated as a "tissue" - a new damping model must be used, as described below.
c    Also note that along with the use of this "nonlinear" material, the output pressure parameter must
c    specify "apres" within the "pout" specification for "pres" (which is a linear parameter when "apres"
c    is not specified) so that the code knows to track nonlinear pressure behavior).
c           prop tmm  1000.0 1561. 0. 0.                    /* previous "elastic" tissue model
c       vdmp tmm  1.105e6 db 0.588  0.0 1.105e6 0.0 0.01   /* previous damping model
c
     type tisu
     wvsp on
     symb alpha = 1.9
     symb exp = 1.25
     symb pmax = 20.e6
     symb pmaxn = -20.e6
     prop tmm  1107.0 1250.0 0.01 0.0 0.0              /* rho measured by Nell; sspd by Dr. Liu
     8.00 $pmaxn $pmax                              /* B/A; pmax, pmin
     sdmp tmm $freq1 db $alpha 0.0 $freq1 $exp 0.01     /* use the "sdmp" damping model for "tisu"
materials
                                        /* attenuation: $alpha*f^$exp dB/cm-MHz
c    Thermal properties (specific heat [J/kg-degC], thermal conductivity [W/m-degC])
c
     thrm watr  4182. 0.60     /* data per ICRU Report #61 (diffusivity = 0.144 mm^2/s)
     thrm tmm   3876. 0.693    /* data measured on 12/19,22,31/08 (diffusivity = 0.16 mm^2/s)
c    thrm tmm   3867. 0.58     /* data per R. King et al. (2007) (diffusivity = 0.15 mm^2/s)

     thrm air   1005. 0.0257   /* data for air per the web
                         /* (diffusivity = 21.3 mm^2/s or ~ 150 times that of water & tmm)

     end

site
     regn watr
     regn tmm   $i2 $i3 $j1 $j3
     regn air   $i3 $i4 $j1 $j3
     end
c
c ******************************** Solution Parameters ****************************
c
heat
     slvr cgds 0.5   /* this is the solver method used in PZFlex example; most efficient
     cupl off
     end

c Define how the heat source is to be applied - for constant sonication for a given
c period of time, define a step function with an amplitude of 1.0 (the actual amplitude
c is provided in the "loss" data file which is read-in below).
c
func step 1.0

c
c Set driving function - on for 1 sec, off for 1 sec, on for 1 sec, then off
c
c data hist drv1 8
c    0.0   1.0
c    1.0   1.0
c    1.001 0.0
```

```
c    2.0   0.0
c    2.001 1.0
c    3.0   1.0
c    3.01  0.0
c  100.00  0.0

symb basetemp = 0.

boun
    side xmin tmpr func $basetemp    /* specify the temperatures at the boundaries to be constant values.
    side ymax tmpr func $basetemp
    side xmax tmpr func $basetemp
    symb scal = $freq1              /* for CONTINUOUS wave problems, scale loss/cycle to power/unit time
by multiplying by frequency
c    symb scal = $prf               /* for PULSED wave problems, scale loss/cycle to power/unit time by
multiplying by pulse repetition rate
    defn heatsource powr func $scal  /* specify the temperatures in the interior to be a heat source ("powr"),
loaded in next line
    mshp sonication.loss loss        /* load the heat source and apply it to the regions sonicated in the
"sonication" simulation
    end

c The following writes-out time-history data to the file "heating.flxhst."
c The file "heating.revinp" is then used to post-process (plot & write text files)
c those time histories.
symb #print on
symb #get { ifocus jfocus kfocus } clsnode $focdist 0.0 0.0
symb #print none
pout
    hist tmpr $ifocus $ifocus 1 $j1 $j1 1          /* temperature at focus (record #1)
    hist tmpr $i3-1 $i3-1 1 $j1 $j1  1
    end

calc
    max tmpr none tmax              /* calculate temperature maxima
    end

c
c Set timestep - thermal is implicit solve, time stability critieria not associated with wave propagation
c Must set small enough to capture temperature change gradients in time.
c
time $tstep

prcs

if ( $graph eq yes ) then
c Display the model prior to execution of the solution
grph
    mirr y
    line no
    nvew 1
    colr tabl matr 5
    map watr 18
    map tmm 10
    map air 26
    plot matr
```

```
    draw node $i2 $i2 $j1 $jndgrd
    draw node $i3 $i3 $j1 $jndgrd
    draw node $i4 $i4 $j1 $jndgrd
    end
endif

c
c ******************************** Solution Execution ******************************
c
set tmpr $basetemp      /* set entire model to base temperature

c
c Apply the heat source and compute; plot temperature each loop
c
symb iendloop = nint ( $sonication_time / $tstep )

c grph              /* IMPORTANT NOTE REGARDING MOVIES (avi files):
c           set imag avi  /* This command sets the image mode to "avi" so that the propagation of the pressure
c           end           /* vave (in the following do loop) can be replayed as a movie.  But, do this only once
                    /* (i.e., outside of the do loop, and do not use "set imag tiff" anywhere else in this file
                    /* because the two formats are not compatible and can not be switched back and forth!

do loop n 1 $iendloop
exec 1              /* for each loop, run simulation for one (1) cycle.
if ( $graph eq yes ) then
grph
           plot tmpr                /* this plots the heating as it conducts
           end                      /* after execution, if needed.
endif
end$ loop

c Write out data for post-processing
c
data
    file out heating.flxout
    out modl
    out tmpr
    out tmax
    end
c Use 'symb #get' function to determine max. value of temperature in the
c model and where it occurs; then write it to the screen and to a file
c

symb #print on
symb #get { temp_max itmax jtmax ktmax } datamax tmpr $i1 $indgrd $j1 $jndgrd 1 1   /* value of max
temperature in entire model
symb #get { x_tmax y_tmax z_tmax } crdnode $itmax $jtmax 1   /* location of max temperature
symb #get { material_tmax } matelem $itmax $jtmax 1          /* find out in which material the max
temperature is found
symb x_tmax = $x_tmax * 100.                          /* convert (x,y) coords from meters to centimeters
symb y_tmax = $y_tmax * 100.
symb #print none


symb #save symb.$labl
stop
```

Appendix B

The inverse technique uses two files written in Matlab. The first file calculates and stores the error for all pairs of W and t_a. This file also passes parameters such as the scaled power value, IR data time shift and also the lowest error between them. The second file is used to plot the input and output traces and display values on screen.

1. Inverse method: MATLAB calculation file

```
format long g
I=AIRC;                    % IR Camera Input file
P=APZF;                    % PZFlex Input file
q=5500;                    % to get power increments in steps of 0.001, ie. (5.5 / 5500)
for m=1:1:(2.2*q);
          for c=1:10              % c is the number of shifts for the IR camera values (on X axis which is also
          the time axis)
      for elem=1:260       % elem is the individual data points
         format long g
         Diff(elem) = (((m/q))*(P(elem)))- (I(elem + c - 1));
         Diff_sqrd(elem) = (Diff(elem))*((Diff(elem)));
         Diff_sqrt(elem) = sqrt((Diff_sqrd(elem)));
         Diff_sqrt_div(elem)=(Diff_sqrt(elem))/sqrt((P(elem)^2));
         Err(elem)= Diff_sqrt_div(elem); % Error for each data point  E= (PZ(i)-IR(i+j))/PZ(i)
      end
   E_int(c,:)=Err;      % Intermediate array with error values for all 260 points.
   end

   for n=10:10:260       % Every 10th point corresponds to a second.. as we have 10 data points per second
      E_next(:,(n/10))= E_int(:,n); % Another intermediate array which has the error values for 1,2,3….26
seconds for all time shifts
   end

   E_n=E_next.'; %The "sum" command in Matlab adds up columns; Transpose required to make columns
contain error for 1,2,3...26 seconds for each shift, for the current power scaled value loop
   format long g
   E_avg = (1/26)* sum (E_n); % Averaged for n = 26
   E_avg_str(m,:)=E_avg;
   fnl_min_avg= min(min(E_avg_str));
   [pvm_val,shft_val,val]=find(E_avg_str==fnl_min_avg);
end
Results1_15(pvm_val,I,shft_val,P,fnl_min_avg)
```

2. Inverse Method: MATLAB results and plot file

```
function [ output_args ] = Results1_15 ( pvm_val,IR_Current,shft_val,PZ_Current,fnl_min_avg)
%This file takes the parameters passed from the Calculation file and plots
```

```
%the traces and also diplays on screen the vales of the lowest error,
%number of times the IR data was shifted and also the scaled value of the
%PZFlex power that gives the lowest error

disp (' ********************PLOT INFORMATION******************** ')

disp (' ')
a1=( (shft_val) - 1 );
if a1==0
IRP=IR_Current(1,1:260);
disp('The IR camera data points have not been shifted because number of shifts = 0 ')
else
IRP=IR_Current(1,(a1+1:260+a1));
disp('The IR camera data points have been shifted these many number of time(s): '), disp(a1)
end
disp (' ')
a2=(((pvm_val(1))/5500));
disp('The scaled PZFlex power value is : '), disp(a2)

disp (' ')
disp('The value of the lowest error is : ') ,disp(fnl_min_avg)
disp (' ')
disp('The row in matrix "E_avg_str" containing the "power multiplier value" for lowest error is : '),
disp(pvm_val(1))

PZP=a2*PZ_Current(1:260);
IRP_trun=IR_Current(1:260);
PZP_trun=PZ_Current(1:260);

timestep=(1:260);
plot(timestep*0.1,IRP,'b-',timestep*0.1,PZP,'r-',timestep*0.1,IRP_trun,'b--',timestep*0.1,PZP_trun,'r--')
title('Optimization curve')
ylabel('Temperature rise in Deg C ')
xlabel('Time (seconds) ')
legend('Time shifted IR data','Scaled PZFLex data','Un-shifted IR data','Un-scaled PZFlex')
axis([0 30 -1 40])
```